Front. Phys., 2013, 8(2): 144–167
DOI 10.1007/s11467-013-0307-y

REVIEW ARTICLE

Properties of SN Ia progenitors from light curves and spectra

P. Höflich[1,†], **P. Dragulin**[1], **J. Mitchell**[1], **B. Penney**[1,2], **B. Sadler**[1], **T. Diamond**[1], **C. Gerardy**[1]

[1] *Department of Physics, Florida State University, Talahassee, FL 32306, USA*
[2] *Department of Physics & Astronomy, Clemson University, Clemson, SC 29634, USA*
E-mail: [†] *pah@astro.physics.fsu.edu*
Received October 5, 2012; accepted December 17, 2012

With recent advances in theory and observations, direct connections emerge between the progenitors of Type Ia Supernovae (SNe Ia) and the observed light curves and spectra. A direct link is important for our understanding of the supernovae physics, the diversity of SNe Ia and the use of SNe Ia for high-precision cosmology because the details of the explosion depends sensitively on the initial conditions and the explosion scenario(s) realized in nature. Do SNe Ia originate from SD- or DD systems, and do they lead to M_{Ch} mass explosions or dynamical mergers? Does the statistical distribtion of SNe Ia depend on their environment which can be expected to change with redshift?

In this contribution, we will exam from the theoretical point of view the tell-tails for this connection, their consistency with the observations, and future directions.

In a first section, we present the physics of the explosion, light curves and spectral formation in a nutshell to help understanding the connection. For details of the progenitor evolution and explosion physics, we refer to reviews and the other contributions in this issue.

Each of the topical sections starts with a brief general review followed by a more detailed discussion of specific results. Because the youth of the field, some bias is unavoidable towards results obtained within our collaborations (and FSU).

The imprint of the metallicity, progenitor stars and properties such as the central density of the exploding WD are presented. IR spectroscopy, polarimetry and imaging of SNR remnants are discussed as a tool to test for the WD properties, magnetic fields and asymmetries. We discuss different classes of Type Ia supernovae, and their environment. Possible correlations between the spectroscopic and light curve properties of SN Ia are discussed. Finally, the overall emerging picture and future developments are discussed.

Keywords supernovae: general, progenitors, light curves, spectra

PACS numbers 98.58.Ay, 98.58.Jg, 98.58.Mj, 98.62.Ai, 98.80.Ft, 98.80.Es

Contents

1 Introduction

Type Ia supernovae (SNe Ia) allow us to study the Uni-

verse at large and have proven invaluable in cosmological studies, the understanding of the origin of elements, and they are laboratories to study physics such as from hydrodynamics, radiation transport, non-equilibrium systems, and nuclear and high energy physics. The consensus picture is that SNe Ia result from a degenerate C/O white dwarf (WD) undergoing a thermonuclear runaway [1], and that they originate from close binary stellar systems. Potential progenitor systems may either consist of two WDs, a so called double degenerate system (DD), and/or a single WD and a main sequence, Helium or Red Giant star, a so called single degenerate system (SD).

Within this general picture, two classes of explosions are discussed which are distinguished by the triggering mechanism of the thermonuclear explosion: (i) One possibility is the dynamical merging of two C/O white dwarfs in a binary system after expelling angular momentum via gravitational radiation. In this scenario, the thermonuclear explosion is triggered by the heat of the merging process. However, it is unclear whether the dynamical merging process leads to an SN Ia, an "Accretion Induced Collapse" (AIC) or a WD with high magnetic fields, and there seem to be too few potential progenitor systems [2–14]. (ii) A second scenario involves the explosion of a C/O-WD with a mass close to the Chandrasekhar limit (M_{Ch}), which accretes matter through Roche-lobe overflow from, for example, an evolved companion star. This is called single degenerate system (SD) [15]. In case of M_{Ch} WD explosions, they are triggered by compressional heating near the WD center. Because the compressional heat release increases rapidly towards M_{Ch}, the exploding stars should have a very narrow range in masses [6]. The donor star may be either a red giant or main sequence star of less than 7–8 solar masses, a helium star, or the accreted material may originate from a tidaly disrupted WD [15, 16]. Throughout this article, we will call the second class M_{Ch} mass explosions which may originate from either SD or DD systems, and dynamical mergers (DM) which may originate from DD systems.

Candidate progenitor systems have been observed for both the SD and DD systems: Supersoft X-ray sources [17–20] showing accretion onto the WD from an evolved companion, and WD binary systems with the correct period to merge in a Hubble time and an appropriate total mass [21]. At least for SN1572, the Tycho SN, the donor star has been identified as a G0 star strongly supporting the single degenerate progenitors [22–24], and two other SNR, 0509-75 & 0519-69.0, favor double degenerate progenitors [25, 26]. Studies have shown that accretion from a Helium star can produce M_{Ch} mass WDs and, based on binary population synthesis, that the Galactic SNe Ia rate is consistent from this channel [27, 28]. Other recent work on rates and the delay time distribution may favor the double degenerate scenario [29–31]. Nevertheless, theoretical work on the explosion, spectra and light curves continues to favor the single degenerate scenario, with some contribution of double degenerate scenario [6, 32–36]. For overviews see Refs. [37, 38], and Refs. [39–41].

From the observation, there are several SD progenitor systems such as super-soft X-ray sources, cataclysmic variables including novae systems and the like. Within the SD evolution, the emerging consensus picture seems to be that these different systems may actually be different evolutionary phases of the same basic system (see proceedings of IAU 281, in press). However, as discussed above, even the evolution of a DD system may lead to M_{Ch} WD explosions if the material is accreted from tidally disrupted WD because the explosion would still lead to a central ignition of a WD close to M_{Ch}. In

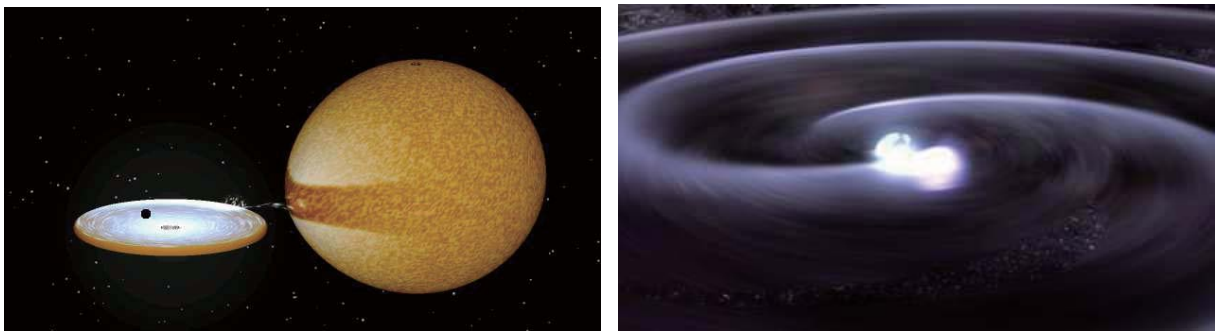

Fig. 1 Artist impression of a single degenerate (SD) and double degenerate System (DD) are given on the left and right, respectively. In an SD system, a single White Dwarf star (WD) accretes from from a Main Sequence Star or Red Giant by Roche-lobe-overflow. The system consists of a WD, the accretion disk, the donor star and wind originating from the accretion disk & donor star and, for high accretion rates, from the WD. Possible systems include cataclysmic variables and supersoft X-ray sources. The image has been produced using the software package simbin-0.8.1 by Hines. Alternatively, possible progenitor systems consist of two WDs, so called double degenerate systems (CREDIT: NASA/GSFC/T. Stromayer). For SD-systems, the thermonuclear explosion of the WD is likely to be triggered by compressional heat when the accreting WD approaches the Chandrasekhar mass, so called M_{Ch} WD explosions. DD-systems may either explode during the dynamical merging of the two WDs or, when one of the WDs is tidally disrupted, as M_{Ch} WD explosions (see text).

contrast, dynamical merging of two WDs will likely result in progenitors with masses ranging from well below M_{Ch} to about 2 M_{Ch}.

The favorable view of M_{Ch} mass explosions as most likely explosion scenario for the majority of SNe Ia is based on the homogeneity in light curves and spectra, though there is strong evidence of contributions of both to the SNe Ia population including $'Super - M'_{Ch}$ mass explosions [6, 12, 42–47]. For reviews, see Refs. [12, 48, 49]. In particular, the chemical structure in the supernovae remnant s-Andromeda and IR line profiles obtained several hundred days after maximum light strongly favor explosions at densities $\leqslant 10^9$ g/cm^3, the hallmark of M_{Ch} explosions [50–54]. Delayed-detonation models [55–57], those possessing a transition from a deflagration to detonation front (DDT) have been found to reproduce the optical and infrared light curves and spectra of "typical" SNe Ia reasonably well, including the time evolution [6, 58–63]. Here the burning starts as a well subsonic deflagration and then turns to a nearly sonic, detonative mode of burning. The amount of burning prior to the transition from deflagration to detonation is the main factor which determines the production of radioactive ^{56}Ni which powers the light curves (see also Refs. [64–66]. When the detonation front propagates through the WD, the density of burning decreases with distance and we see a layered chemical structure consistent with observations in both the abundance pattern and velocity distribution of individual objects [6, 42, 58–63, 67–69]). The brightness decline relation (Δm_{15}) relates the absolute brightness at maximum light and the rate of the post-maximum decline over 15 days. The Δm_{15} relation plays a key role both for cosmology and understanding of the explosion physics [70–72]. From theory, Δm_{15} is well understood: LCs are powered by radioactive decay of ^{56}Ni [73]. More ^{56}Ni increases the luminosity and causes the envelopes to be hotter. Higher temperature means higher opacity and, thus, longer diffusion time scales and slower decline rates after maximum light [74–77]. Δm_{15}-relation holds up for virtually all explosion scenarios as long as there is an excess amount of stored energy to be released [74, 78]. The tightness of the relation observed for Branch-normal SNe Ia is about 0.3^m [71, 79–82], consistent with explosions of models of similar mass, but hardly consistent with the entire range of masses for two WDs undergoing dynamical merging. However, M_{Ch} explosions have their problems too. Although, the brightness of the relation can be understood within the framework of the single degenerate scenario and spherical delayed detonation models [68, 74, 83], it falls apart when taking into account burning instabilities and mixing during the deflagration phase [64, 74, 77, 84]. Some important piece of physics appears to be missing still which may restore a "close-to-1D" nature.

For M_{Ch} explosions, some progress has been made in understanding variations among SNe Ia, with suggestions that some of the spectral diversity is due to metallicity, central density, WD rotation and asymmetries [42, 54, 83, 85–91]. It is widely accepted that pre-conditioning of the WD is a key solving the problems of current explosion models and understanding the diversity in SNe Ia [50, 64, 77, 78, 90, 92–102].

A set of extremely bright SNe Ia may lend support for dynamical merging with progenitors well above the Chandrasekhar mass [43, 103–105]. We note, however, that the inferred brightness depends on a unique relaton between the ^{56}Ni mass M_{Ni}, and the intrinsic color B-V at maximum light. At least, in a few cases, the apparent brightness can be understood within the framework of M_{Ch} mass WDs with an intrinsically red color rather than a boost in brigthness by assuming a large interstellar reddening correction [44].

Another probe for the progenitor systems is the environment of SNeIa which will shed light on the evolutionary history of the progenitor by modifying the supernovae light curves (LCs) and spectra. Hydrodynamical impact of the SN ejecta will produce additional emission and may modify the outer structure of the envelope and, thus, the Doppler shift of spectra features. Light emitted from the photosphere of the supernovae may heat up matter in the environment which, in tern, may change the ionization balance or the dust properties.

So, from theoretical explosion models, both M_{Ch} mass explosions and dynamical mergers seem to have problems to provide a consistent picture. We miss important physical effects in the explosion or the progenitor paths. On the other hand, due to advances in observations, it becomes evident that we are starting to actually see the signatures of the progenitor systems in the light curve and spectra of supernovae. However, the interpretation of individual observables may not be unique in light of the unknowns. We need to connect those constrains and weight highest observational characteristics which do not depend sensitively on details.

In this contribution, we will discuss some possible links between theoretical signatures and the observations, and will try to develop a consistent picture and discuss the current limits and future possible paths. In the first section, we will discuss the basic physics of the explosions and the environment to lay the groundwork for the interpretation of the physics of the explosion, light curves and spectra. In the subsequent chapters, we present the links i) between secondary parameters of the LCs and the primordial metallicity, central density and the main sequence mass of the exploding WD, with ii) the late

time light curves and IR spectra to decipher the central density and magnetic field of the WD and, finally, iii) observable signatures of the progenitor system's environment.

2 Thermonuclear supernovae in a nutshell

Explosion: The basic concept of the explosion is rather simple. Carbon ignition leads to a thermonuclear runaway in the WD because the degenerate electron gas shows hardly any temperature dependence. A nuclear burning front propagates through the WD which has a radius of about 1500 to 2000 km and a binding energy of about 5... 6×10^{50} erg. Burning of about 1.4 $M_\odot$ of a C/O-rich WD releases about 2×10^{51} erg in nuclear binding energy which is used to overcome the binding energy of the WD and causes its complete disruption on a time scale of seconds. As a result, we see a rapidly expanding envelope consisting of the burning products. The exact amount and products of the nuclear reactions depend mainly on the time scale of reactions compared to the hydrodynamical time scale of expansion, which is ≈ 1 s. Though the individual reaction rates depend sensitively on the temperature and density, overall, the final burning products depend mainly on the amount of available fuel per volume which is a function of the density and, to a smaller extent, the initial chemical composition, namely the C/O ratio of the progenitor. The structure of a typical SNe Ia model is shown in Fig. 2. At densities $\geqslant 2 \times 10^7$ g·cm^{-3}, temperatures exceed 5×10^9 K and the matter is burned up to nuclear statistical equilibrium. Elements of the iron-group are produced. At densities $\geqslant 4 \times 10^6$, and $\geqslant 10^6$ g·cm^3, the matter undergoes incomplete Si-burning and explosive O-burning which produce mainly S/Si and Ne/Mg/O, respectively. Within each group of burning products, the isotopic composition is close to a quasi-NSE [106]. To first order, the isotopic composition depends on the electron/baryon ratio Y_e which is inherented from the progenitor for all layers but those with densities $> 10^9$ g·cm^{-3} where electron capture becomes dominant. For SNe Ia, the main question is how individual mass elements are burned, and their distribution in the envelope. For dynamical mergers of low or higher mass, the initial conditions scale according to the mass. For dynamical mergers, a relatively low density, intermediate state is formed which produces intermediate mass elements without a deflagration phase, and ^{56}Ni down to the center.

For M_{Ch} models, the most likely scenario are the delayed-detonation models [57, 107]. The delayed detonation model assumes that burning starts as a subsonic deflagration with a certain speed $S_{\rm def} < c_s$, and then undergoes a transition to a supersonic detonation with a speed $D > c_s$ (DDT). During the deflagration phase, the WD expands which, mainly, depends on the amount of burning during the deflagration phase. The transition of the burning to a detonation occurs when the rate of burning increases sufficiently to ignite the unburned matter by compression. For WD conditions, a nuclear detonation wave will propagate once initiated. Possible mechanisms which cause the DDT are still under discussion and include the Zel'dovich mechanism, i.e., mixing of burned and unburned [108, 109], crossing shock waves produced in the highly turbulent medium, or shear flows of rising bubbles at low densities [49, 88, 89, 94, 96, 110], and instabilities in the regime of distributed burning [66] causes the transition from a deflagration to a detonation front. Note that the properties of pure deflagration models contradict the observations which require vanishing amounts of unburned matter and, by and large, radially-layered chemical structures [58, 60, 62, 66–69, 111–113]. Even for delayed detonation the question remains how to suppress large scale mixing during the deflagration phase (see below).

Light curves and spectra: What we observe is not the explosion itself but light emitted from the material of the disrupted white dwarf (WD) for weeks to months

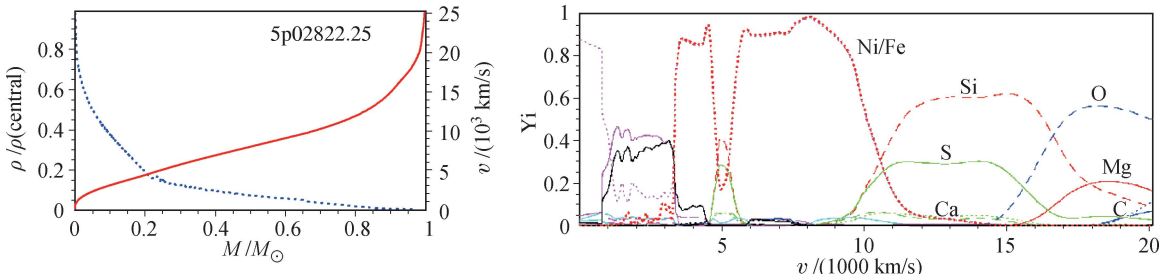

Fig. 2 Structure of a spherical delayed detonation model which can reproduce LCs and spectra which originates from a progenitor with a main sequence mass of $5M_\odot$ and solar metallicity [68]. Density (*blue, dotted*) and velocity (*red, solid*) as a function of the mass are given on the left. Abundances of the most abundant stable isotopes as a function of the expansion velocity are given on the right. In the center, the abundances correspond to ^{54}Fe, ^{58}Ni and Co. We note that current 3D calculations predict similar structures but with strong mixing of large fractions of the envelope. Strong mixing is inconsistent with observations (see text).

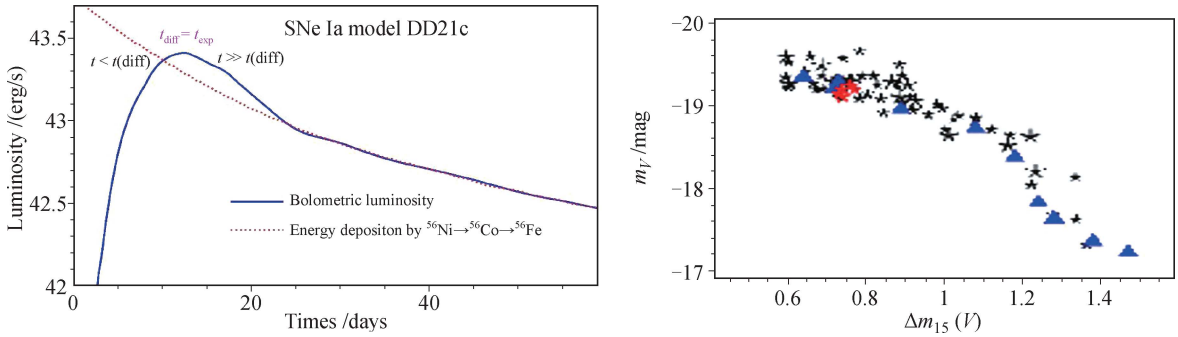

Fig. 3 Schematic light curves of SNe Ia (left) and the $\Delta m_{15}(V)$ (right) of 66 well-observed SNe Ia [81, 114, 115] in comparison with theoretical values for delayed detonation models [68] which are based on the same progenitor model but differ in the amount of burning prior to the DDT. For the transformation between $\Delta m_{15}(B)$ to $\Delta m_{15}(V)$, see Ref. [116].

afterward. After the first few seconds, this rapidly moving gas expands freely. As a consequence, the matter density decreases with time and the expanding material becomes increasingly transparent, allowing us to see progressively deeper layers. A detailed analysis of the observed light curves (the time series of emitted flux) and spectra reveals the density and chemical structure of the entire star.

- Spectra measure the decoupling region of the optically thick and thin region, the so-called photosphere, at a certain time. Spectral lines allow identification of elements. Line profiles are governed by the Doppler shift and, thus, the time evolution probes the chemical and density structure of the envelope.
- Bolometric and broad band light curves mostly depend on the balance between the energy input and cooling by expansion, and diffusion time scales. They are sensitive to the inner layers below the photosphere.

A schematic bolometric light curve is shown in Fig. 3. To first order, the curve can be understood by the competition between the time-scales of the hydrodynamics causing the expansion and the diffusion of the energy via radiation transport. The optical depth of the envelope decreases with the expansion, i.e., $t(diffusion) \propto t^{-2}$. Typically, the optical depth of SNe Ia envelopes are about 30 at maximum light, i.e., 15–20 days after the explosion [58, 117]. Two to three months after the explosion, radiation transport effects become small and diffusion time scales become short compared to the expansion times. At this time the bolometric curve is given by the instantaneous energy input. It is dominated by the radioactive decay and the escape probability for hard γ-ray photons and positrons.

For cosmology the relation between the absolute brightness and the decline rate (Δm_{15}) plays a key role [70–72] (see Fig. 3). From theory, Δm_{15} is well understood: LCs are powered by radioactive decay of ^{56}Ni [73]. More ^{56}Ni increases the luminosity and causes the envelopes to be hotter. Higher temperature means higher opacity and, thus, longer diffusion time scales and slower decline rates after maximum light [68, 74–77]. The existence of a Δm_{15}-relation holds up for virtually all scenarios as long as there is an excess amount of stored energy to be released [74]. The tightness of the relation can be understood within the framework of the single degenerate scenario and spherical models [68, 74, 83], and it falls apart when taking into account burning instabilities during the deflagration phase [77]. For a tight Δm_{15} relation, SNe Ia with similar ^{56}Ni should encounter similar amounts of mixing. The quantitative agreement of the spherical models shown in Fig. 3 is only possible because spherical models suppress mixing. ^{56}Ni layers are increasingly confined to the central layers of the WD with decreasing mass of 56Ni. This is consistent with the observation that the mean half width of Fe/Co/Ni lines decreases with brightness [118].

Observed SNe Ia envelopes seem to show similar overall structures because the physics demands so and not (!) necessarily because they are a homogeneous class of objects with respect to the progenitor evolution, the thermonuclear runaway and explosion because nuclear physics leads to a "stellar amnesia":

- Type Ia supernovae light curves are nearly homogeneous because nuclear physics determines the structure of white dwarfs, and the explosion.
- The total production of nuclear energy is given by the total amount of burning. It is almost constant since very little of the WD remains unburned. The final explosion energy depends on the binding energy of the WD, which is given by its structure.
- The light curves are powered by the radioactive decay of ^{56}Ni → ^{56}Co → ^{56}Fe produced during the explosion, rather independently from details of the explosion physics and progenitors. The amount of ^{56}Ni determines the absolute brightness.
- The amount of ^{56}Ni determines the heating. More heating means higher temperatures and higher opacities.

- Higher opacities imply longer diffusion time scales and, consequently, a slower release of energy stored during the pre-maximum phase during which the envelope is optically thick and the diffusion time-scales are longer than the time since the explosion. Consequently, energy stored at earlier times is released slower and the decline rate becomes smaller with increasing ^{56}Ni (as long as excess energy is stored at previous times see text and Section 5).
- Eventually, the envelope becomes optically thin and the decline of the LC is determined by the nuclear decay rate and the escape of the radioactive energy.
- To agree with observations of intermediate mass elements at the outer layers, the M_{Ch}-mass WD must be pre-expanded. Most likely, an initial deflagration phase causes the pre-expansion. This depends mainly on the amount of energy release but not on the details of the deflagration front.

Despite the overall "stellar amnesia", some progress has been made in understanding variations which we will address in the following sections.

3 Light curve indicators for the metallicity, central density and main sequence masses

The brightness-decline relation for SNe Ia light curves [70] has been well established as a cornerstone of modern cosmology [71, 79, 80, 82]. As a result, the light curves are self-similar within ±0.3 mag [119, 120] and the transformation to a template light curve can be described by the rate of the decline past maximum light, Δm_{15} [71], or by stretching the time-axis by a factor s [119, 120]. The stretching method works for both the local and high-z samples [121, 122]. The self-similarity holds even for supernovae for which super-Chandrasekhar mass progenitors have been suggested (see Section 1).

Only during the last 15–20 years, advances in observations and computational methods allow detailed studies of secondary effects by accessing the information needed (e.g., Ref. [123]). Information is provided by physical laws and relations used in the models, and observational constraints. Constraints are provided by i) information on individual objects based on flux and polarization spectra and their evolution with time, and the morphology of SN remnants, ii) statistical properties such as the brightness distribution within the same class of objects and, iii) integrated quantities such as the chemical composition in our galaxy.

Some actual progress has been made in understanding variations among the SNe Ia, with suggestions that some of the spectral diversity is due to different progenitors, explosion scenarios, metallicity, central density, rotation and other asymmetries [54, 77, 83, 85, 86, 90, 124–126]. The data base for well observed supernovae have been greatly enhanced by recent supernovae searches including Carnegie Supernova Project (CSP) [127–129], CfA3 [130], Supernova Factory [131], etc. CSP allowed high precision differential light curves between supernovae pairs and lead to the discovery of signatures which may be attributed to the main sequence mass of the progenitor WD and the central densities [83].

Subsequently, this analysis was generalized and applied to the entire set of CSP data [132]. We want to discuss this analysis in more detail because the CSP data are publicly available. In future, other data sets will provide similar accuracy on larger samples.

3.1 Analysis of light curves of the CSP supernova sample

The results below are based on 25 high precision UBV light curves of the Carnegie Supernova Project, with a good coverage of maximum light. The LCs are highly uniform with an accuracy of a few hundredth of a magnitude both for individual SNe Ia and in terms of variations between different objects [127–129]. As discussed above, variations in the progenitor's Main Sequence Mass (M_{MS}), the central density of the WD at the time of the explosion (ρ_c) and the progenitor metallicity (Z) all play a role in the intrinsic diversity of SNe Ia on top of possible deviation from sphericity. The analysis below is novel but based on several prior findings:

– The brightness decline relation can described by a stretch factor s in time [119], and the stretch mostly depend on the amount of ^{56}Ni produced (see Section 1). The visual light curve V resembles the bolometric light curve and, thus, the maximum brightness M_V correlates with ^{56}Ni.

– The V light curve around maximum light (between −5 and +15 days) hardly depend on variations in the the central density and the chemical C/O structure of the progenitor, i.e., its main sequence mass and Z [85, 133]. However, we expect a strong peak to tail variation. It is crucial to determine the stretch s from a well defined time interval.

– metallicity variations Z include two main effects, namely i) the change of nuclear burning and a shift of nuclear quasi-equilibria from ^{56}Ni to non-radioactive nuclei of the iron-group by a shift of the electron to nucleon ratio Y_e and ii) change of the opacities. The former effect is mostly caused by the enrichment of the protostellar cloud by ^{22}Ne produced in massive stars when the progenitor was formed [85, 134]. The pre-mordial Y_e mostly affects the actual value of s.

Based on detailed spectral calculation, it was found

that opacity changes due to Z will have strong affect on the U and the UV and, somewhat, the B band but hardly V and IR magnitudes [85, 133]. The models also predict little influence of ρ_c and M_{MS} on the LC shapes around maximum light.

– the central density of the exploding WD and M_{MS} by changing the C/O ratio in the WD affect the ratio between the peak brightness and the tail of LCs because the impact on the ^{56}Ni production in the center and the explosion energy [85]. From the observations, variations of the peak to tail ratio have been established [127, 128] and the differential light curve signatures predicted have been found [83].

3.1.1 Primary parameters

As a first step, s and the time of maximum light are determined by using the visual light curves for the CSP SNe. Subsequently, theoretical templates for the differentials between two supernovae are used to determine the secondary parameters. In a first step, the individual light curves have been corrected for redshift, the k-correction. The differentials are obtained by substracting the stretched light curves which have been normalized to maximum light. For details, see Refs. [135, 136].

The stretch factor s is used as primary parameter to transform the light curves to a standard template. V has been used in a defined time interval between -5 to $+15$ days for reasons mentioned above. The s-values agree well with the reduced time-range provided by Kriscuinas [132] and, for the extended range, with SNooPY [137]. Note that a limited and well defined interval in time is crucial because we expect peak to tail variations [138].

3.1.2 Secondary parameters for ρ_c, M_{MS} and the metallicity

Component analyses is used to study n secondary parameters in a specific wavelength band. The differences $\Delta m(t)$ in LC pairs are described by

$$\Delta m_{ij,obs}(t) = \sum_{k=1,n} \lambda_k(ij) f_k(t) + Res_{ij}(t)$$

with $\lambda_k(ij)$ being the coefficients for a pair of SN i and j, $f_k(t)$ the principal components, and $Res(t)$ the residuals. The Downhill–Simplex method [139] is used to find the $\lambda_k(ij)$, i.e., to minimize the residuals. The Simplex Method is a multidimensional minimization allgorithm. From the CSP data base, we include 25 SN, i.e., 300 pairs. Only 25*n $\lambda_{ij} = g_k(i)/g_k(j)$'s are independent where $g_k(i)$ is the eigenvalue of f_k to be attributed a specific SNe Ia. The overdetermined system is solved using QR or LQ factorization. The $g_k(i)$ can be related to physical quantities based on models.

To study the influence of the initial main sequence mass M_{MS} of the progenitor and the central density ρ_c of the progenitor, V is used because the shape of the LCs hardly depends on Z. Depending on the details of the geometry, aspherical density structures may produce an LC signature which is morphological similar to the ρ_c signatures. However, the interpretation of a ρ_c variation is supported by the the IR-spectra and supernova remnants as discussed in Section 4.

U is very sensitive to the metallicity and, at maximum light, shows variations up to 1.3 magnitudes for the same stretch s [140]. This variation masks the other secondary parameters.

In Fig. 4, the templates are given based on theoretical models [49, 85]. M_{MS} (and, somewhat metallicity changes Z) will change the C/O ratio in the WD because the sensitivity on the central He-burning during the normal stellar evolution [141, 142]. A lower C/O ratio means less energy release during the explosion, and a smaller expansion rate. Δm rises slower due to the smaller geometrical dilution. Secondary "dips" are seen around 30 days past maximum light in V and are caused by the photosphere entering the ^{56}Ni deficient core. Eventually, Δm becomes close to zero when all instant energy deposition contributes to the LC. Variations in ρ_c mostly affect the size of the core region with little or no ^{56}Ni. Because expansion and diffusion time scales are both about equal at maximum light for models with the same stretch s, the inner region does not contribute to the brightness. However, at later times, lesser ^{56}Ni results in an off-set. Note that asymmetries may be produce a similar offset when the envelope transitions from the optically thick to the transparent phase but the transition should be expected somewhat later and slower. Similarly, For U, a Z-change leads to an off-set at about maximum light (Fig. 4, right panel) mostly due to the changes in line blocking by lines of the Fe-group elements. About 1–2 weeks after maximum light, the photosphere is formed in layers of complete burning which are dominated by Fe-group elements regardless of Z. As a consequence, two models are hardly affected by Z at late times. B and R show the same trend with V however, less accurate. B depends on asphericity and Z [126] and Z [85], and its residuals depend more sensitively on uncertainties of maximum light. R shows a significant the strength of the secondary maximum.

Results: Some examples are given in Fig. 5. SN2004ef, SN2005al, SN2005iq, SN2005am, SN 2005na are Branch-normal SNe Ia and have stretch factors s of 0.84, 0.89, 0.86, 0.73 and 0.95, respectively. The pairs SN2005al/SN2005am, SN2004ef/SN2005el, SN2004ef/SN2005na and SN2005am/SN2005iq are given

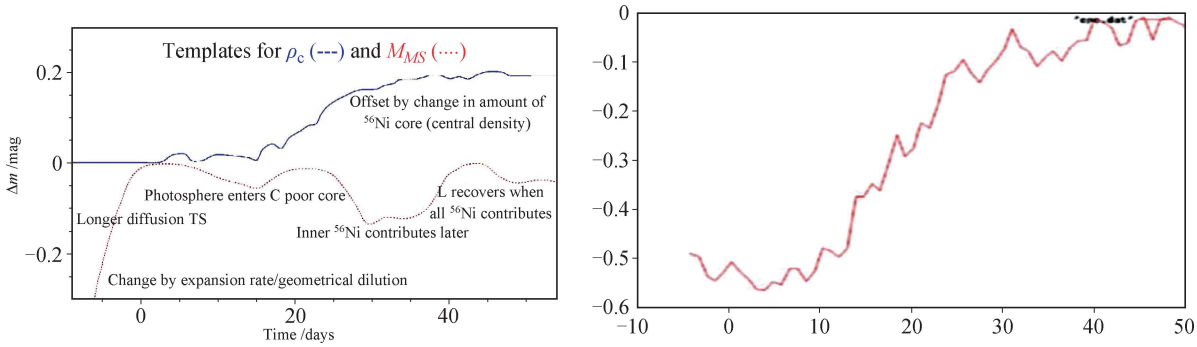

Fig. 4 Principal components (PC) in V (left) and U (right) based on theoretical models (see text and Ref. [132]). For U, the component has been recalibrated using a PC analysis of observations. We show the difference in V brightness $\Delta m(t)$ (in magnitudes) as a function of time (in days) relative to a reference models with solar metallicity and a main sequence mass M_{MS} of $5M_\odot$ and a central density of the exploding WD of ρ_c of 2×10^9 g·cm^{-3}. The annotation at the graphs give the main cause for the difference for the V light curves. From the models, the PC in U can be understood as result of the pre-mordial metallicity Z. Early on, blocking of iron lines depends strongly on Z because it is formed in the layers of incomplete burning whereas, at later times, the photosphere is formed in layers of complete burning where most of the matter is burned to Fe-group regardless [85].

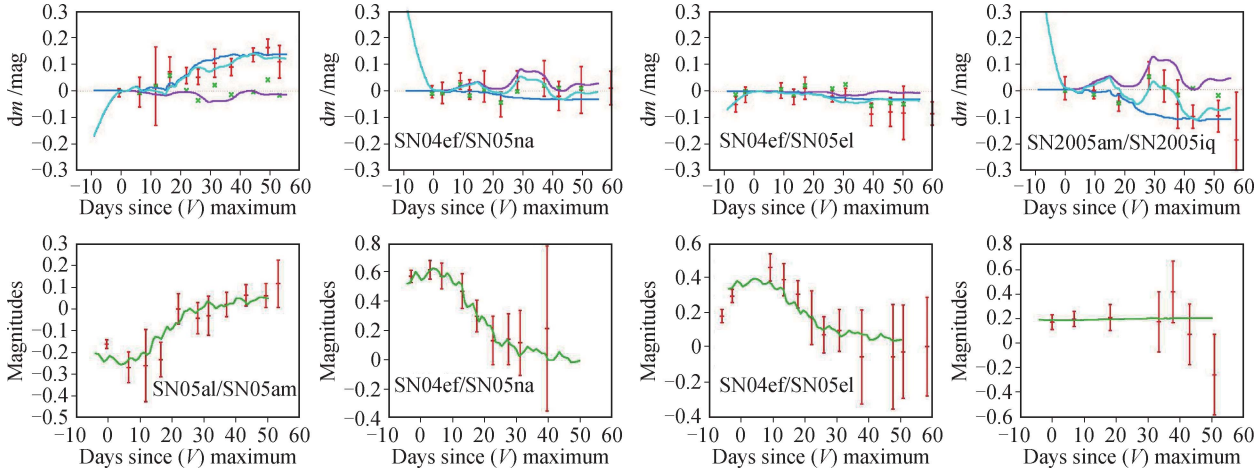

Fig. 5 Best fits to the observed differential dm of individual pairs of SNe Ia by the PCs in V (upper) and U (lower), respectively. The differential brigthness has been obtained after normalization to the same stretch s. For V, we give the weighted components (blue and magneta) and their sums (cyan) along the observations (with error bars). In addition, the residuals are given (green crosses). The examples have been choosen to for pairs which are dominated by differences in the central density, the main sequence mass, small differences and a mixed case (from left to right). Note the varying scale of the y-axes. The residuals are small and, within the error bars, consistent with zero. For U, we give the metallicity component Z, only. Its amplitude is up to $\approx 1^m$ in the CSP sample and, thus, dominates the secondary components. Note that the U component may not go to zero which can be attributed to interstellar reddening, and s variations [132].

for $\tilde{\lambda}_{ij} = g_i/g_j$ in which g_i are the properties of an individual supernova. The pairs are examples of supernovae which differ mostly in ρ_c, M_{Ch}, are very similar and differ in both ρ_c and M_{MS}, respectively. Using theoretical templates seems to work and reduces the residuals based on stretch from ≈ 0.3 by an order of magnitude. Overall, the residuals are consistent with zero within the error bars in both U and V which may lend support for using model templates. From the theoretical models, M_{MS}, ρ_c and Z are independent parameters because they depend on the progenitor WD, the accretion rate and, thus, the donor star as it fills the Roche-Lobe, and the premordial matter from which the systems has been formed. However, $\tilde{\lambda}_{ij}$ are not necessarily unique due to errors in brightness and time coverage in several cases (see Fig. 6). Moreover, similar relations may be produced by other effects and even within the dynamical mergers. For example, off-center ^{56}Ni or asphericity mergers may produce templates with similar patterns to ρ_c and Z. Although asphericity should act similarly on the ρ_c and Z signals and our examples, e.g. SN2005am/SN2005iq, do not show this pattern, and it may still contribute to the combined signals and, moreover, our sample of SNe is small. We note that all pairs of SN1991t-like objects show $\lambda(ij) = 0$ in all components. Within the picture of M_{Ch} explosions and classical delayed-detonation models, either they are very similar despite differences in Δm_{15}, or they lack a central region of high densities and have similar C/O progenitors. How-

ever, we may want to mention two alternatives: Within the M_{Ch} picture, SN1991t-likes may originate from explosions which undergo a strong pulsation prior to the DDT, the so-called pulsationg delayed detonation models [6], which results in strong mixing of the inner layers. Within the picture of dynamical mergers, similar mixing may be induced. Note that dynamical mergers may show to the signatures of M_{MS} and the ρ_c signature may be mimiced by asphericity effects which may be probed by spectro-polarimetry as mentioned above. For more details and a complete analysis of all CSP SNe Ia, see Refs. [132, 136].

Statistical properties: As mentioned above, the number of SN-pairs far exceeds the number of free variables which allows the reconstruction of $g_k(i)$s. Remapping the individual $g_k(i)$ to M_{MS}, ρ_c and Z allows us to study the distributions (Fig. 7): (a) ρ_c are distributed from 1×10^9 g·cm^{-3} to 7×10^9 g·cm^{-3}, i.e., close to the accretion induced collapse (AIC) (b) SN Ia come from massive progenitors with $M \geqslant 4M_{\odot}$ and (c) most of the progenitors at low redshifts cluster around 0.03 to 1 times solar metallicity. A very small fraction show metallicities well in excess of solar.

Correlations: In Fig. 8 some of the correlations between ρ_c, M_{MS} and Z are given as a function of redshift and stretch s, i.e., the absolute brightness. There are no correlations seen with redshift because the CSP SNe are all at low redshifts z ($z \leqslant -0.1$)/ This provides a test for consistency of the data set including effects of the k-corrections and reddening. Although small, the CSP sample is suggestive that low luminosity SNe Ia may originate from low metallicity and, possibly, low density WDs. We may see a hint that subluminous SNe Ia have very long evolutionary time scales which is also consistent with the apparent lack of SN1991bg-like objects in high redshift samples.

As mentioned above, the residuals in the LCs are reduced by an order of magnitude compared to a one-parameter fit. Potentially, secondary parameters may allow high-precision cosmology but the accuracy must still be tested from observations of supernovae at larger redshifts to eliminate peculiar velocities of the galaxies.

4 Central densities and magnetic fields from spectra and supernovae remnants

As discussed above, one feature of M_{Ch} mass explosions are the high central densities which leads to the production of non-radioactive iron-group elements than ^{56}Ni (see Fig. 2). In the previous section, we identified the possible signatures of high central densities in the visual light curves but noted that asphericity may have a similar effect because the directional dependence of the luminosity may be significant early on but will decrease at later times when most of the ^{56}Ni-rich layers become transparent [58, 87, 91, 143]. In a first part, we want to present evidence for high central densities from IR-spectra during the nebular phase and supernovae remnants. In a second part, we want to present possible

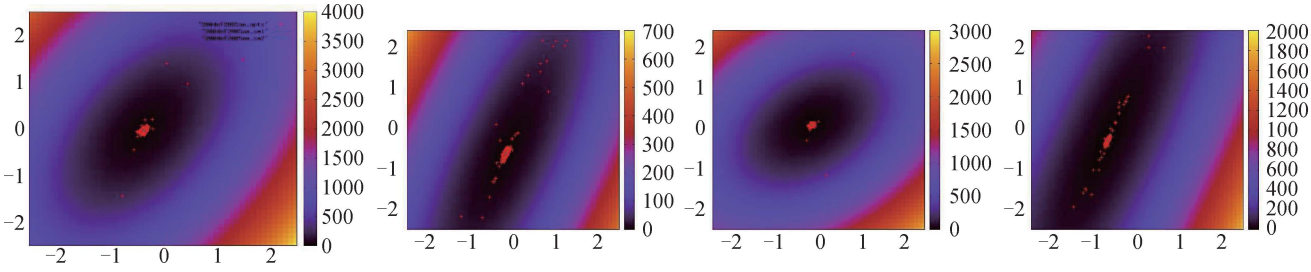

Fig. 6 Likelihood distributions of $\tilde{\lambda}_{ij}$ for the same SN-pairs as in Fig. 5 based on MC solutions for the overdetermined system. The x- and y-axis correspond to the progenitor and central density parameter, respectively. In some cases, sparse time coverage produce large uncertainties in the eigenvalues.

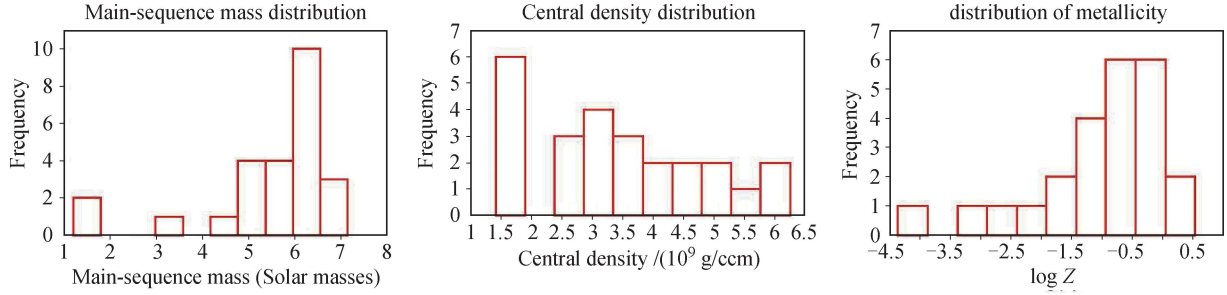

Fig. 7 Distribution of main sequence masses of the progenitors, the central density of the WD at the time of the explosion, and the metallicity. Note that the current data allow to identify trends but the error bars are quiet large for individual SNe Ia (see Fig. 5).

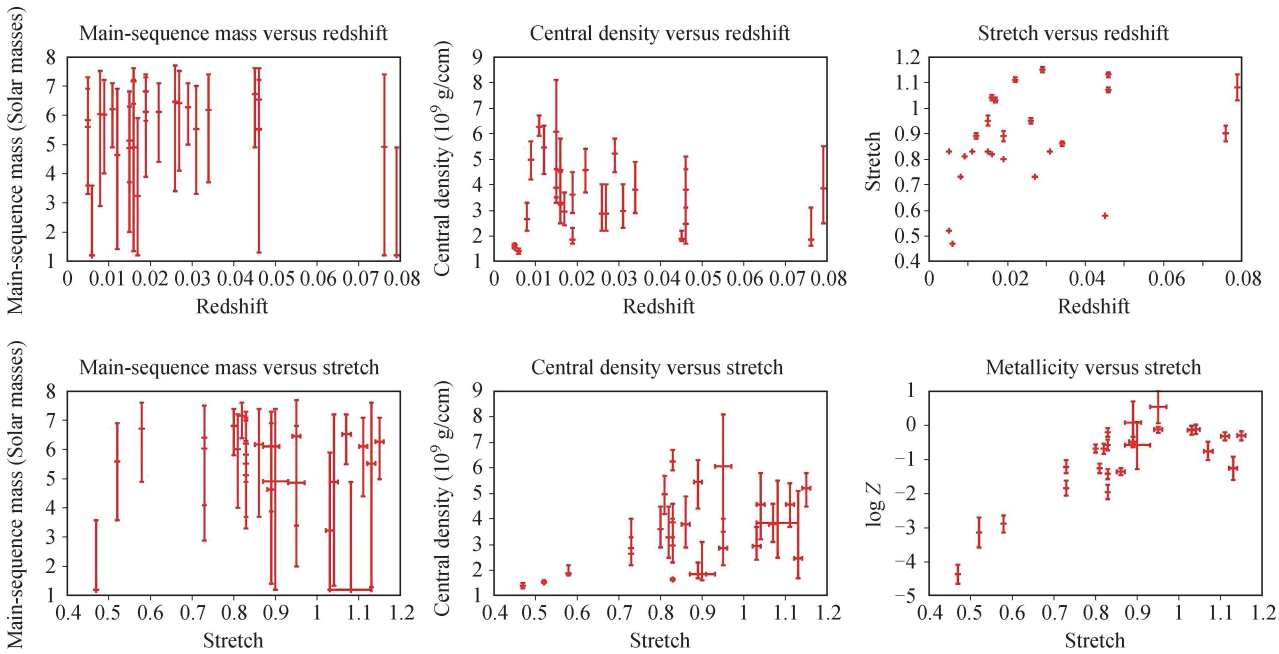

Fig. 8 Correlations $F(x)$ for supernovae in the CSP sample, and the slope based on a regression analysis. There is no signifanct correlation between M_{MS}, ρ_c and s as a function of redshift (upper row). This is expected because small range in redshift. Correlations between the intrinsic parameters M_{MS}, ρ_c and Z as a function of s (second row) show slopes of 0.42 ± 1.27, 4.0 ± 1.314 and 5.07 ± 0.89, respectively. We note that $M_{MS}(s)$ shows a fast drop at the low end of s in the first sample of the CSP data. Most of the SNe Ia with large uncertainties are the sample obtained in 2006/7.

evidence for magnetic fields which are sufficiently large to effect the thermonuclear runaway.

4.1 Evidence for high central densities

When the ejecta are optically thin and the spectra are dominated by Fe-group elements, nebular phase spectroscopy of SNe Ia in the optical and infrared (IR), can be used to reveal the structure at the center of the explosion [50, 51, 53, 54, 144]. The forbidden [Fe II]-line at 1.65 μm is almost unblended and, thus, allows a direct measurement of the distribution of Fe which is excited by the nuclear decay of ^{56}Ni $\rightarrow ^{56}$Co $\rightarrow ^{56}$Fe, namely the β^+-decay channel of ^{56}Co. Note that all γ-rays produced during the decay can escape freely (see below). Comparison between the observed spectra for SN 2003du and SN 2004hv are given in Fig. 9. The line at 1.65 μm shows particular line profiles with flat top and asymmetric wings indicating material with a central cavity and some central off-set. Note that identical profiles and features have been observed in the mid-IR by the Spitzer Space Telescope for the same (and other) supernovae which lends support for the geometrical interpretation. In SN2003du and SN2005hv, the profiles show asymmetries in the line wings to the red and blue, respectively. These asymmetries can be understood in the framework of off-center DDT models seen from different angles [126, 144]. Both the flat top and its width is consistent with spherical DD models which inhibit mixing due to Rayleigh-Taylor instabilities and (!) assume local energy deposition by positrons [50, 144]. Based on simple approximations, Höflich et al. estimated that the initial magnetic field in the WD must be larger than 5000 Gauss [50].

Independent from the interpretation of line profiles, the direct imaging of the Supernovae-Remnant *s*-Andromeda provides additional evidence for both a central cavity in ^{56}Ni and off-center DDT M_{Ch} mass explosions. The remnant of SN1885, S-Andromeda, was discovered by Fesen when he obtained images in several lines with the Hubble Space Telescope [145–147]. S-Andromeda is a unique remnant because its vicinity to the galactic center of the Andromeda galaxy produced a sufficiently low density environment that the SN envelope is still expanding freely even after more than 125 years. The historical light curve and the chemical distributions have found to be consistent with a slightly underluminous SNe Ia similar to SN1986g within the picture of M_{Ch} mass explosions [52]. In Fig. 10, we give the distribution of elements as observed and as expected from models. The lack of Ca in the center indicates high density burning and little mixing because Ca is destroyed in high density burning (see Fig. 2). Explosion models with Ca in the center produce centrally peaked images closely matching the density structure inconsistent with the observations. In contrast, the Fe emission is centrally peaked because, at that time, we have ^{54}Fe or ^{56}Fe in the

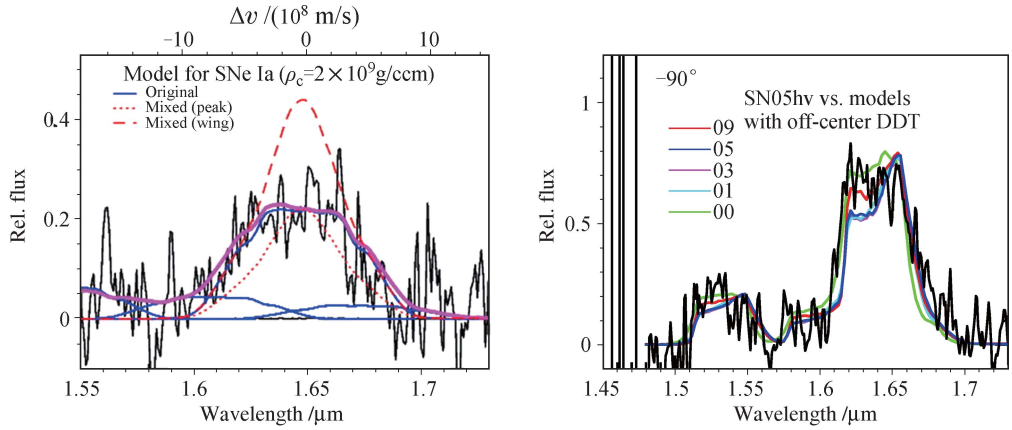

Fig. 9 Infrared line profiles of SN 2003du and SN 2003hv taken with the Subaru telescope at about 300 and 390 days after the explosion, respectively, in comparison with various predicted line profiles by delayed-detonation models. On the left, the solid line is the predicted relative flux of the forbidden Fe II transition at 1.644 μm for a delayed detonation model (*solid*) with little mixing. The two dotted lines are with a mixed chemistry with the smaller dotted line being fitted to the observed peak, and the dashed line being fitted to the observed wings. The weaker contributions from the minor Fe II lines are also visible (1.599, 1.664 and 1.677 μm). On the right, the comparison of SN2003hv is given to DD models seen in which the DDT was triggered opposite to the line of sight at distances between 0.1 and 0.9 of the WD radius. The lack of emission at close to the rest velocity of the SN is indicative for the explosion of a WD close to M_{Ch}. Line asymmetries in the wing supports off-center DDTs [49–51].

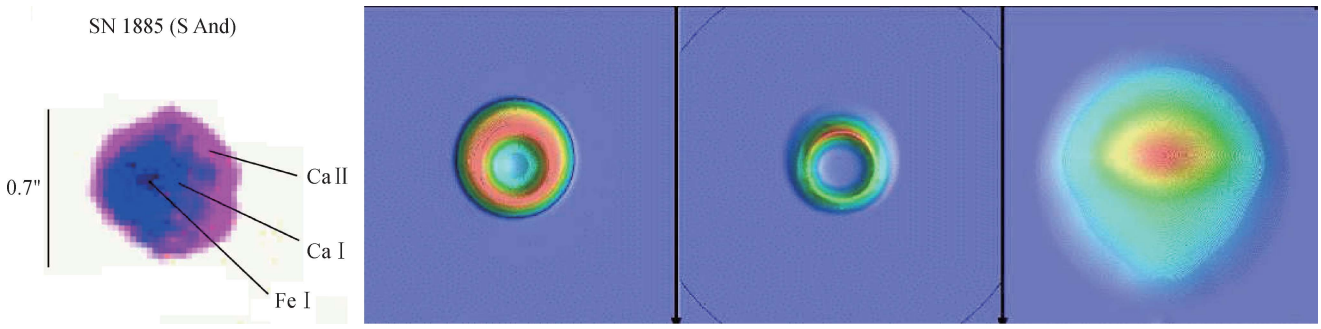

Fig. 10 Images of the remnant *S*-Andromeda observed with ACS/WFC at HST and modeled in the lines of CaI (at 4227 Å), CaII (*H&K* at 3950 Å) and Fe I (at 3300 Å). Ca II shows a ring of 11 000 km/s radius, Ca I shows part of a ring off-center by about 3000 km/s. Fe I is centrally peaked as can be expected from the density and chemical structures. The theoretical images for CaII, CaI and FeI (*right plots*) are based on a detailed ionization model for an off-center DDT (Reproduced from Ref. [52]). Note that, in the models, the *y*-axis is the direction of symmetry.

center in, basically, all explosion scenarios. Central densities in dynamical mergers are lower compared to M_{Ch} mass explosions and current models citebenz90, kmh93, hk06, guer04, Garcia07, pakamor11, pakamor12 tend to produce Ca in a narrow velocity range or show central Ca. However, results depend sensitively on the mass ratio of the WDs. S-Andromeda lends support to the explosion of WD with high central densities such as M_{Ch} mass WD coming either from an SD or DD scenario but disfavors dynamical mergers with a low mass. Note, however, that we see no or little evidence for chemical mixing predicted by 3D deflagration models.

The picture of high central densities of the WD is common and is supported by light curves, late time IR spectra and, in one case, direct imaging of a supernova remnant.

4.2 Evidence for high magnetic fields

For the interpretation of the IR line profiles, one of the key assumptions was that the positrons are locally trapped and that the profiles trace the combined effect of the distribution of radioactive elements, namely ^{56}Ni, and of the Fe-group elements.

Several authors have addressed the transport of positrons [148, 149]. Early papers [150, 151] used one-dimensional approximations and assumed the magnetic field was either chaotically twisted at a scale small enough to trap the positrons in place or radially combed by the expansion, so that the positrons were forced to move radially. They neglected the matter interaction of the positrons and, thus, overestimated the positron diffusion but showed that energy deposition by positrons

dominate late time light curves of SNe Ia. These analysis lead the way to measure magnetic fields B by late time light curves. Lower B means an increase escape fraction for positrons and, thus, a steeper decline of late time light curves. Subsequent studies [152] have improved on the positron transport using detailed cross-section and Monte-Carlo technique but continued to use either a 1D radial magnetic field, and applied it to SNe Ia light curve. The results presented below [153, 154] are based on a very similar method but assuming initial dipole fields of a strength B at the polar surface. Here, the B-field has radial and transversial components. The results are similar to Milne *et al.* But, in general, the escape probability is slightly lower. The escape fractions of γ-rays and positrons and the relative contribution to the relative energy input by γ photons is shown in Fig. 11. The resulting V light curves are shown in Fig. 12. Energy input by γ rays dominate during the first 3 months. However, due to the small cross section for high energy photons compared to positrons, positrons start to dominate the energy input and power the light curves after a few months. After about one year, positrons start to escape depending on the magnetic field. The late time light curves the energy input can change by factors. Thus, late time visual light curves provide a tool to determine even moderate initial B fields on the level of 10^4 G. In practice, one problem is that the escape of positrons depends sensitively on details of the models such as mixing of ^{56}Ni and asymmetries. Light curves don't provide sufficient observables to separate the effects.

Late time IR-spectra can overcome this problem. In particular, the mid-IR forbidden Fe II-line at 1.65 μm (see above) provides direct information about the energy input by radioactive decay via the Doppler shift (see above). More precisely, the Fe II IR line emission provides information about the region where we have

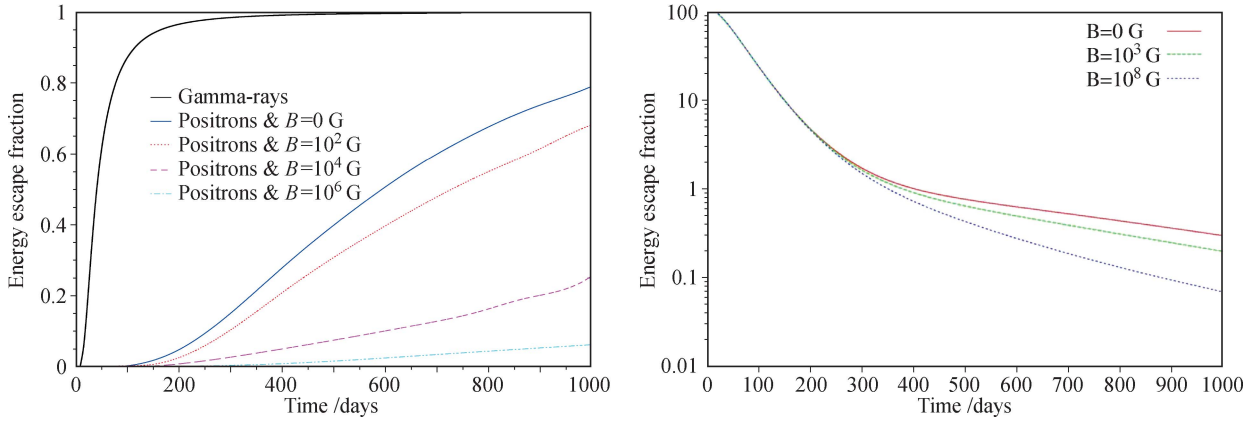

Fig. 11 Gamma- and positron escape fractions for the energy produced by the decays ^{56}Ni $\rightarrow^{56}$Co $\rightarrow^{56}$Fe with time for B-fields of $0, 10^4, 10^6$ and 10^8 G (*left*), and the fraction of γ-rays relative to the combined energy input by γ-rays and positrons (*right*). We use a typical delayed-detonation model (Fig. 2). Here, dipole fields are assumed of strengths B at the polar surface of the initial WD, and that the field is frozen-in the expanding material.

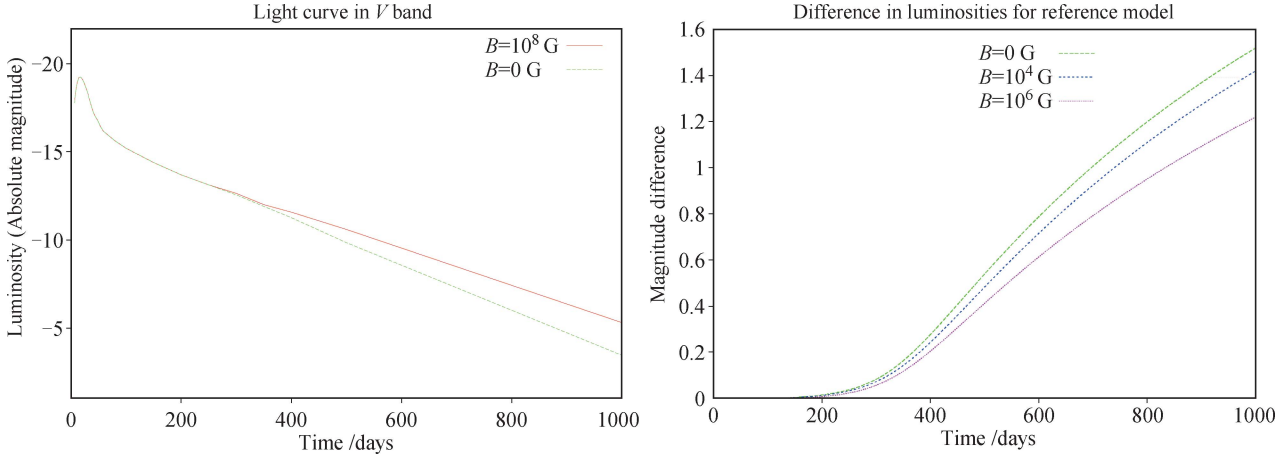

Fig. 12 V magnitudes luminosity in V of a typical delayed-detonation model with no magnetic field ($B = 0$ G) and a strong 10^8 G field (*left*). On the right, we show the difference between the models of $B = 0, 10^4, 10^6$ with 10^8 G as a baseline. Note that positrons are mostly locally trapped at 10^8 G.

iron and (!) energy input by γ-rays and positrons. Recently, detailed Monte-Carlo calculations for positron transport have been performed for different classes of SNE Ia for a wide range of explosion models including detailed calculations for the IR-line profiles [135, 153, 154]. In Fig. 13, the energy deposition by positrons is given as a function of time and the strength of the magnetic field B. The change of the energy input can be understood by the increasing free mean path of positrons as a function of the decreasing density structure of a typical SNe Ia (Fig. 2). The free mean path of positrons increases with increasing velocity, time and the size of the magnetic field (see Fig. 13).

As discussed above, line IR profiles provide a direct link to the local energy input as a function of velocity, and the distribution of elements. Line profiles allow to decipher the 3D signature of the envelope when taking into account the evolution of the optical depth with time. The evolution of the IR-line profile at 1.65 μm is shown in Fig. 14. Up to about 100 to 150 days, the energy input is dominated by the deposition of γ-rays which does not depend on the magnetic field. Because γ rays penetrate to the center and excite the central iron, the line profile is peaked and off-set due to an optically thick core

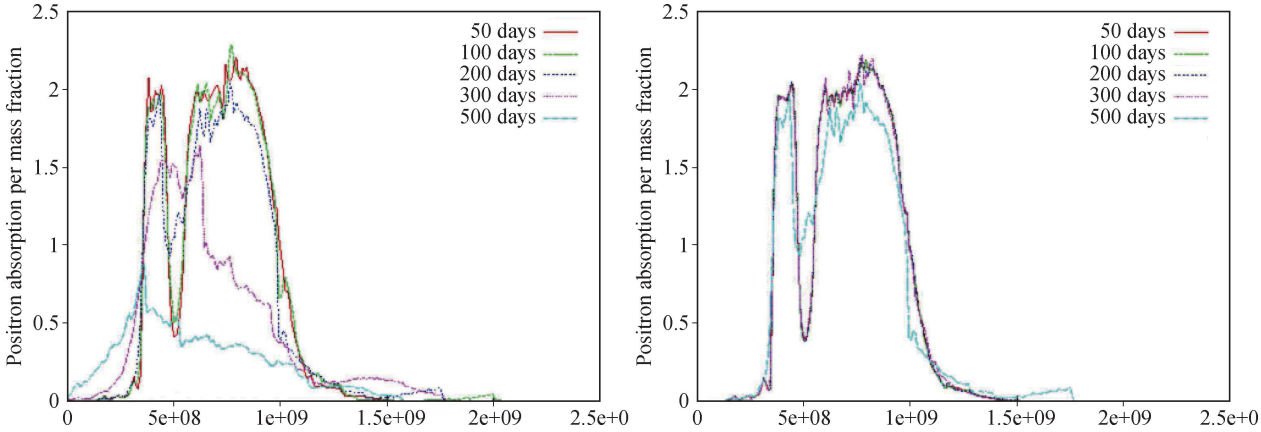

Fig. 13 Positron absorption per unit mass as a fraction of total instantanious energy input by radioactive decays for a typical delayed detonatin model (see Fig. 2) for $B = 0$ and 10^8 G. Lines for 500 days are multiplied by a factor of ten. At early times the effect of the positrons are small compared to γ rays, but after $\approx$ 100 days, the energy input (see Fig. 11).

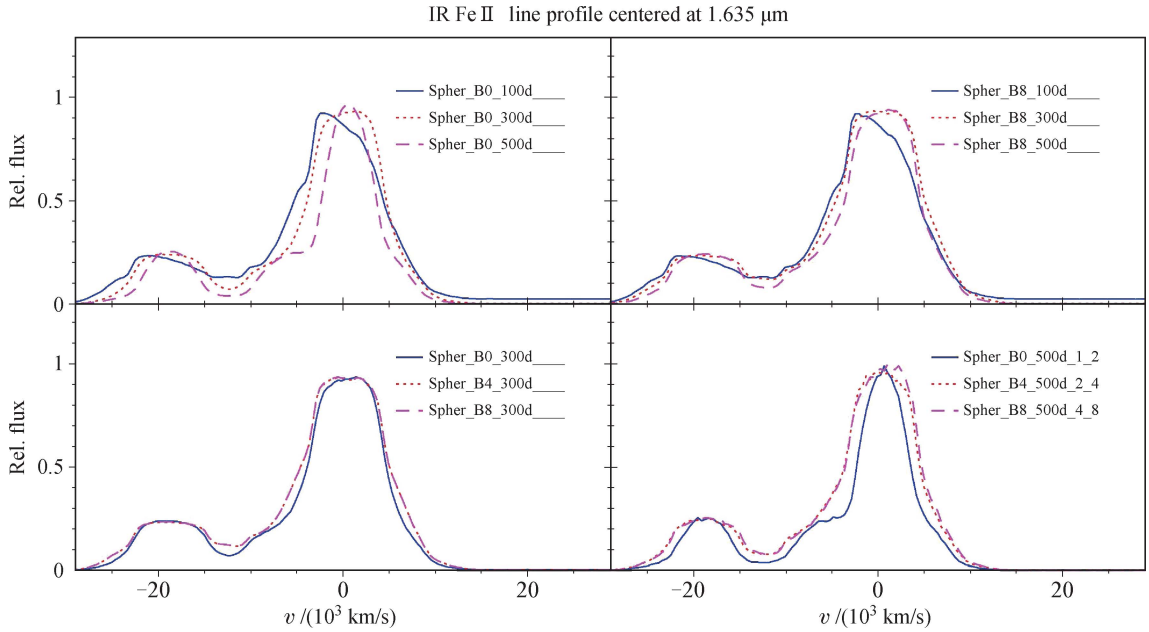

Fig. 14 Profiles of the forbidden IR Fe II lines at 1.635 μm for various times and magnetic fields B using a delayed-detonation model (Fig. 2). We assume dipole fields of strengths B at the polar surface of the initial WD and followed its evolution that it is frozen-in the expanding material. The time evolution of the profiles are shown for $B = 0$ G (*left*) and $B = 10^8$G (*right*) in the upper panels for days 100, 300 and 500 after the explosion. Note that spectra up to about $\approx$ 200 to 300 days are affected by optical depth effects and, consequently, blueshifted [153]. The lower panels show the effect of the magnetic fields of 0, 10^4 and 10^8 G at day 300 and 500. Note that the time evolution of the profiles is needed to separate optical depth effects, asymmetric distribution of ^{56}Ni and the B field (see text).

consistent with the observations [155]. Subsequently, positrons dominate and, from the chemical structure, we expect profile with flat top and width of $\approx$ 3000 km/s and $\approx$ 6000–9000 km/s (see Fig. 2). Note that optical depth effects in the envelope will shift the velocity offset in lines and change the morphology up to about 200 to 250 days. At day 300 and beyond, positrons dominate the energy input and they start to redistribute the energy. Line profiles vary with the size of the magnetic field B. To be consistent with the flat-top of SN2003du and SN2004hv [50, 51], B fields in excess of $10^{4...6}$G are needed, respectively. B fields of this size are interesting because the Lorenz force is comparable to the pressure gradient dP/dr in the initial WD [92, 102, 156] and may affect turbulent field build up during the thermodynamical runaway and, in the presence of large passive flows, evolution of the flame during the deflagration phase.

5 Odd-balls and other clues

The majority of SNe Ia appears to be homogeneous. They can be used as "standard candles", and some 90% fall within the narrow class of "Branch-normal" or SN1991bg like events [157]. However, some clearly fall out of the sequence of the brightness decline relation and spectroscopic properties which can be understood in terms of ^{56}Ni mass and temperature.

SN1991t-like: This class of objects represents about 9 % of all SNe Ia. Its brightness is at the upper end of 'Branch normals' with a low Δm_{15} [158, 159], and comparably weak layers of intermediate mass elements [160–164]. The spectra and light curves are very similar and, as discussed in Section 3.1.2, they do not show evidence for secondary parameters (Ref. [135], see Section 3). Moreover, late time spectra do not show "peaked" late time IR, i.e., ^{56}Ni is found up to the center [155] which is consistent with the lack of a signal for ρ_c.

SN2000cn-like: This class of objects shows very high ionization in their spectra unlike subluminous supernovae but, similarly, steep declines post maximum. Late-time light curves are comparable to very lower end of "Branch-normal" SNe Ia. The high ionization may be a hint for interaction.

Hyper-Chandra explosions: The observation of a set of extremely bright SNe Ia may lend support for double degenerate scenarios with progenitors well above the Chandrasekhar mass [43, 103–105]. We note, however, that the assumption on the inferred brightness depends on a unique relation between the ^{56}Ni mass $M_{\rm Ni}$, and the intrinsic color B–V at maximum light. At least, in a few cases, the apparent brightness can be understood within the framework of M_{Ch} mass WDs with intrinsically red color [44].

SN2001ay-like objects: This class shows that nature is even more diverse. SN2001ay declines slower than any SNe Ia known combined with a fast rise of some 16 days and shows a blue color [165]. SN2001ay would be brighter by about 1^m based Δm_{15} and the distance to the host galaxy. In fact, Δm_{15} is slower than implied by the instant energy input by radioactive decays $\dot{E}_\gamma$. It was suggested [166] that SN2001ay is merger originating from a super-Chandrasekhar mass WD. However, the mass required for the slow decline is in excess of 3 M_{Ch} masses and which is well above the limit for mergers which is given by $2 \times M_{Ch}$. Alternatively, this SN can be still be understood within the physics underlying the Δm_{15} relation, and in the framework of pulsating delayed detonation models originating from a M_{Ch} mass WD but with a core of some 80% Carbon instead of the 15 to 20% usual for stellar central He burning [78, 135]. Higher carbon fraction means more nuclear energy by ^{12}C$(\alpha,\gamma)^{16}$O by about 40% and faster expansion of the inner layers. Faster expansion means i) a larger fraction of the energy by ^{56}Ni decay goes into expansion work rather than boosting the luminosity at maximum light, ii) lower optical depth and iii) shorter rise time. In those models, the maximum brightness is smaller than the instant radioactive energy release $\dot{E}\gamma$ (Ref. [167]), and the light curves approaches $\dot{E}\gamma$ "from below". This model agrees reasonable well with the observational light curves and spectra. The reason for a high C abundance remains speculative. During central He burning, a star produces high C abundances during the early ^{4}He burning but, under He-deleted conditions at the end, ^{12}C$(\alpha,\gamma)^{16}$O depletes C unless strong mixing of He avoids this phase. A possible path may be a common envelope like in the progenitor of SN1987A.

In Fig. 15, the theoretical LCs in B and V are compared with the observations. The agreement is reasonable, and they meet the brightness limit imposed by the early non-detection in R. The theoretical B and V have been corrected for the redshift z of the host galaxy. As discussed in the introduction, the distance modules of the host galaxy is 35.5 ± 0.1 mag, and the galactic foreground extinction $E(B-V) = 0.026$ mag. Ref. [165] use a reddening of the host galaxy of $E(B-V) = 0.072$ mag with an R_V of 3.1 and 2.4 for the Galaxy and host galaxy, respectively, giving $A_V = 0.253$ mag. Using the theoretical color $(B-V)_{max} = 0.0$ mag and from an an optimized fit, the host galaxy reddening would be $E(B-V) = 0.02$ mag with a global $R_V = 3.1$ for a total extinction $A_V = 0.144$ mag.

For a consistent absolute V magnitude of -19.2 mag, the resulting synthetic spectrum is compared to the spectrum observed at maximum light in Ref. [78]. The

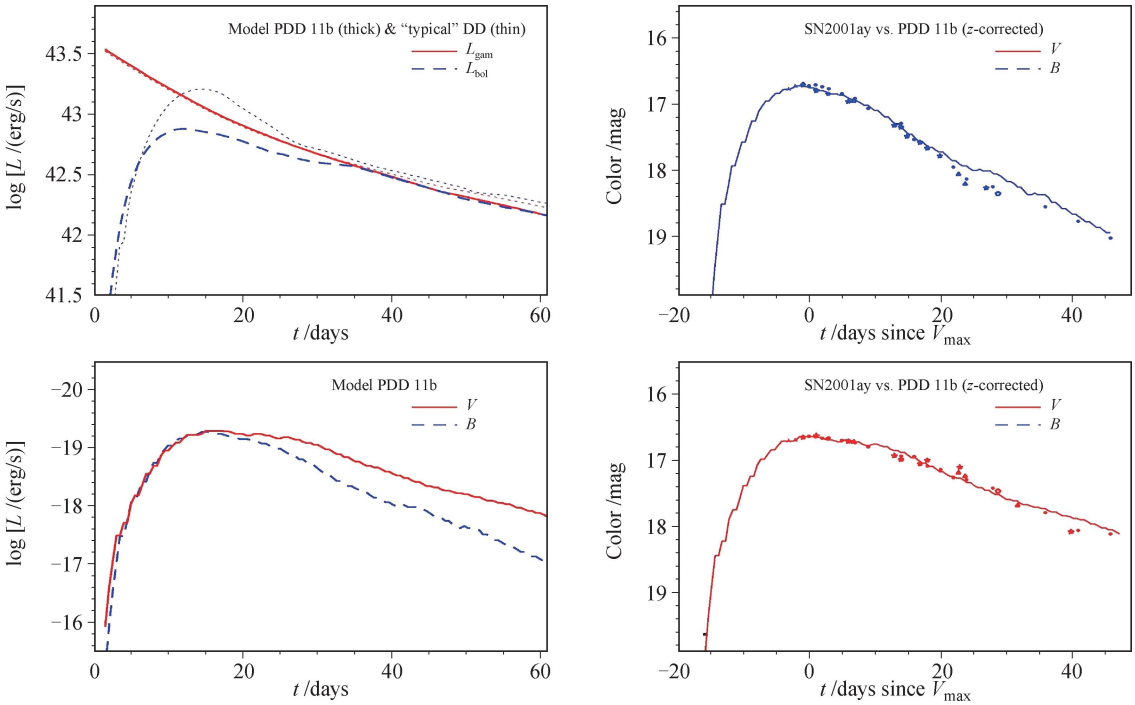

Fig. 15 B and V LCs of SN2001ay [165] in comparison with theory. We give the instantaneous deposition by radioactive matter for PDD11b [78, 135], a pulsating model with a carbon rich core, and a "classical" delayed-detonation model (upper left), and the B and V (lower left). The energy input of the delayed-detonation model has been scaled by 0.037 dex to equal the gamma-ray input at maximum light. SN2001ay and PDD11b are compared in B (upper right) and V (lower right) as a function of time since maximum light in V observed. The model lightcurves have been correct for reddening and redshift. A distance module $m - M$ and total reddening $E(B - V)$ have been assumed to be 35.65 mag and 0.096 mag, respectively.

continuum colors are well reproduced. The synthetic value of B–V equals 0.07 mag, fully consistent with 0 mag of SN2001ay.

The maximum spectrum is dominated by single ionized lines of S II, Si II, Ca II, Fe II, Co II as well as blends of double ionized species in the blue. The synthetic and observed spectra show agreement. The Doppler shifts of lines from elements undergoing incomplete oxygen burning include the Si II λ6355, Si II λ5970 and S II. Ca II H+K and the IR triplet are well reproduced with 10, 20 and 30 Å, respectively which which corresponds to a difference velocity shift of 500 up to 1000 km/s at measured velocity of 14 400 km/s. The strength of the absorption components agree well. Some disagreement is evident. The blue component of the S II W at about 5000 Å is too weak and, in the blue, blends due to Co II are too strong, including a feature at 7400 Å. For the same reason, the emission component of the Si II λ6355 is suppressed by absorption of Co II. Likely, the Co II emission is also responsible for the apparent weakness of the blue component of the S II W. For more details, see Ref. [78].

6 Environment of Type Ia supernovae

In the previous sections, we have addressed several aspects of the progenitors. The environment must be expected to depend on the properties of the progenitor system (Fig. 1), and the scenario must be consistent with the lack of ongoing interaction observed. A noticeable exception is SN 2002ic which shows spectra closely resembling a normal SN Ia, but it also exhibits H lines similar to those seen in SNe IIn with both broad and narrow components. Significantly more than $0.1 M_{\odot}$ of H-rich material is required to explain the features in SN 2002ic, with the H-rich gas at distances between 10^{16}–10^{17}cm. This matter might be attributed to a short period of high mass loss in a binary system or during a planetary nebula phase several thousand years before the explosion [168–170]. The high mass loss may be explained by a system with an initially rather massive donor star ($M_{MS} \approx 3 M_{\odot}$) which has experienced a delayed dynamical instability [171]. The same mechanism may also account for SN2005gj, another another 2002ic-like object [172].

As discussed below, the density limits for the environment of a typical SNe Ia are well below those of the solar neighbourhood and the goal of this section is to discuss whether SD and DD systems may create this environment.

In case of DD progenitors Fig. 1, we may expect long evolutionary time scales and, likely, the binary system

has moved far away from its place of birth and the stellar evolution prior to the WD stage. Any circumstellar material at large distances should be uncorrelated to the DD system. In most cases, we may expect a low density environment consistent with observations.

The environment of SD systems can be expected to consist of three main components: i) Some matter bound in the progenitor system at the time of the explosion. It may originate from the accretion disk and be shed from the donor star; ii) the wind from the WD, accretion disk and donor star, and iii) the interstellar medium (ISM).

There is clear evidence for interaction with the matter within the progenitor system. Within the explosion of M_{Ch} mass WDs, hydrodynamic calculations have shown that the expanding supernova material wraps around the companion star and may pull off several tenths of a solar mass of material [77, 173]. Another sources of matter is the accretion disk [53] matter lifted during a pulsational phase during the explosion or debris from the merging of two WDs [6, 174]. There has been some evidence indeed for interaction between the explosion and the environment. Although H-lines like in SN 2002ic are rare, a common feature in almost all SNe Ia is a high-velocity Ca II line which, first, was prominently seen in events like SN1995D, SN 2001el, SN2003du, and SN 2000cx, a feature present in almost all SNe [53, 133, 174–176] and which may be attributed to the material of even solar metallicity bound or in close proximity of the progenitor system (see Fig. 16).

At intermediate distances of up to several light years and in case of M_{Ch} mass explosions, the environment may be dominated by the wind from the donor star, the accretion disk or, for high accretion rates, by the wind from the WD, or the interstellar material (ISM). A number of possible signatures of the interaction has been studied, including X-rays, in the radio and narrow H and He lines but no evidence has been found with limits of $10^{-5} M_{\odot}$ for the mass loss [177–181]. In late-time light curves, interaction should result in excess luminosity but no sign of an interaction has been found even in SN1991T which has been observed up to day 1000 which implies densities lesser than $\approx 10^{-3}$ particles/cm^3 [182].

At large distances, namely beyond a few tenth to several light years, the environment is determined by the ISM. It is known that Type Ia SNe generally explode in low density environments away from the high densities of star forming regions [183]. This can be partly attributed to the long stellar evolutionary lifetimes of the low-mass stars in the progenitor systems, affording them ample time to move away from their place of birth. SNe Ia occur in elliptical and spiral galaxies including galactic disks, the bulge and the halo. One may expect the explosion to happen in densities of $\approx 10^{-3...10}$ particles/cm^3 (e.g. Ref. [184]). Indeed, extinction laws seem to be different from the interstellar medium in our galaxy suggesting a component linked to the environment of SNe Ia rather than the general host galaxy [185–189]. Light echos from SNe Ia have been used to probe the environment of SNe Ia and showed that many SNeIa have circumstellar dust shells at distances of a few up to several hundred parsecs [172, 190–195]. Most evidence of a link between SNe Ia and their environment comes from the observations of narrow, time-dependent, blue-shifted Na D absorption line which, for a significant fraction of all SNe Ia, indicates strong outflows [196–199].

The following picture of the environment emerges:

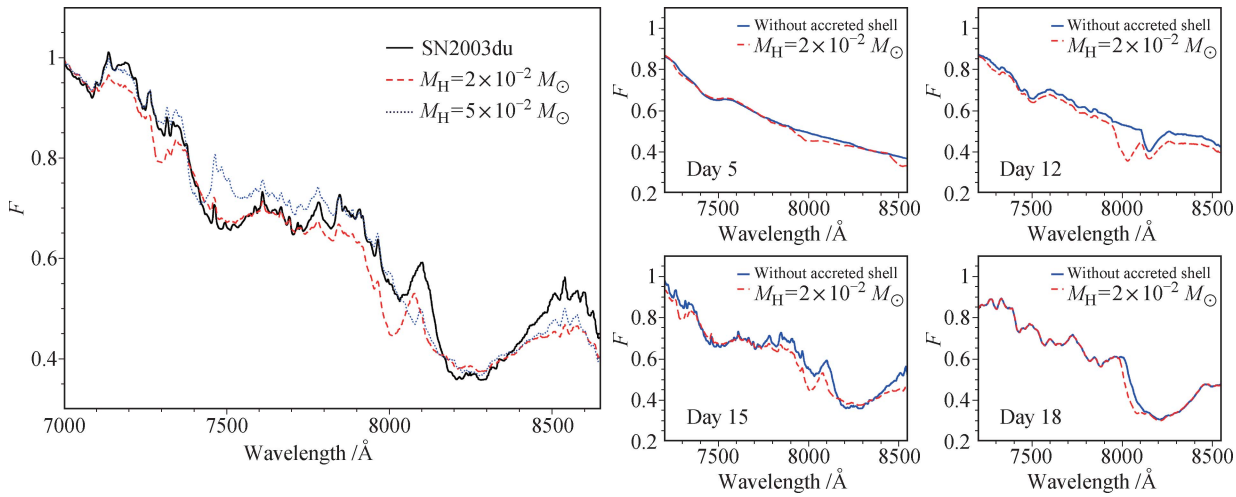

Fig. 16 The high-velocity feature of Ca II as observed in SN2003du some 3 days before maximum light in comparison to a delayed-detonation model with about $2 \times 10^{-2} M_{\odot}$ of solar metallicity. On the right, we show the spectral evolution with time between day 5 to day 18 for the model without and a shell with $2 \times 10^{-2} M_{\odot}$. The dominant signature of interaction is the appearance of a secondary, high velocity Ca II feature or, for high shell masses, a persistent high velocity component in a broad Ca II line which starts to appear at about 5 days after the explosion (Reproduced from Ref. [53]).

SNe Ia are surrounded by a cocoon with a much lower density than the ISM often, separated by a higher density region which produces NaD and may contain dust.

6.1 A simple models for the progenitor/environment interaction

The current state of the research leaves some important questions unresolved. How can we understand the low density environment and the general structure? Which of the wide variety of progenitor systems are compatible with the observations and the range of parameters? What other possible signatures might be seen due to the interaction of the explosion within the possible progenitor systems?

These questions have been addressed in a recent paper (as part of a PhD thesis) which employed spherical, semi-analytical models constructed by piecewise, scale-free analytic solutions similar to Parker's solution [200, 201]. Scales enter the system via the equation of state, the boundary and jump conditions. For details, see Ref. [202]. The free parameters are: i) The velocity v_w and ii) mass loss rate $\dot{m}_1$ from the central object, and the iii) $n_o = const$ (Table 1) or iv) a mass loss rate $\dot{m}_1$ with $v_{w,1}$, i.e., $n \propto r^{-s}$, and iv) the duration of the wind interaction t_w (Table 2). As a result, we obtain the density, velocity and pressure as a function of time, namely $\rho(r,t), v(r,t)$ and $P(r,t)$ which can be attributed to observables. Parameters have been used which correspond to different regimes (see Tables 1 and 2). Typical structures are seen in Fig. 17. The structures are characterized by i) an undisturbed, inner layer dominated by a fast wind, ii) an inner, shocked region with almost constant, low density, and a velocity declining with distance, iii) an slowly expanding shell of high density of "swept up" material expanding at a typical of 10 to 100 km/s and, iv) the ISM. A low density bubble with $\leqslant 10^{-3...-5}$ g/cm^3 has been formed with a radius of about 10...100 ly. However, its size depends on the duration of evolution t, i.e. the accretion rate. Increasing the accretion rate by a factor of 100 reduces the bubble size to a 1/10th of light year. In that case, we may see hydro interaction with the dense shell within 1 to 3 years.

In the tables, some typical structures are given for winds running into an environment of densities = *const* and $\propto r^{-2}$. For accretion disk winds the mass loss rate

Table 1 Wind interaction with a constant density ISM ($s = 0$) for the accretion disk wind (models 1–7) and an RG wind originating from "over Eddington" accretion or a RG donor star (models 8–12). The first 7 models correspond to the wind from the accretion disk Values for the radial distance of the contact discontinuity, outer shock front, inner shock front, and density at the inner shock front calculated from the given outer density, wind speed, wind mass-loss, and run time. Densities are given in particles per cubic centimeter. The 3000 km/s velocity corresponds to the accretion disk wind case and the 30 km/s velocity is for RG wind.

n_0/cm^{-3}	v_w/(km/s)	$\dot{m}/(M_\odot/\mathrm{yr})$	t/yr	R_c/ly	R_1/ly	R_2/ly	ρ_2/cm^{-3}
0.100	3000	10^{-8}	3×10^5	34.4	40.1	5.13	1.9×10^{-5}
1.00	3000	10^{-8}	3×10^5	21.7	25.3	2.57	7.5×10^{-5}
10.0	3000	10^{-8}	3×10^5	13.7	16.0	1.29	3.0×10^{-4}
1.00	3000	10^{-9}	3×10^5	13.7	16.0	1.29	3.0×10^{-5}
1.00	3000	10^{-10}	3×10^5	8.64	10.1	0.646	1.2×10^{-5}
1.00	3000	10^{-8}	1.5×10^5	14.3	16.7	1.95	1.3×10^{-4}
1.00	3000	10^{-8}	4×10^5	25.3	30.0	2.88	5.9×10^{-5}
0.100	30	10^{-7}	4×10^7	163	190	45.7	2.4×10^{-4}
1.00	30	10^{-7}	4×10^7	103	120	22.9	9.4×10^{-4}
10.0	30	10^{-7}	4×10^7	64.8	75.5	11.1	3.7×10^{-3}
1.00	30	10^{-6}	2×10^6	27.0	31.4	13.8	2.7×10^{-2}
1.00	30	10^{-8}	6×10^8	329	383	33.9	4.3×10^{-5}

Table 2 Interaction the accretion disk wind (model 1–7) with a RG wind originating from the progenitor WD exanding in a low density environment ($v_{w,1} = 30$ km/s, $v_{w,2} = 3000$ km/s, $s = 2$). Models 8–12 show the same environment but for the case of a RG wind from "over-Eddington" accretion. Values for the radial distance of the contact discontinuity, outer shock front, inner shock front, and density at the inner shock front calculated from the given outer wind mass-loss, inner wind mass loss, and run time. The outer wind speed is 30 km/s and the inner wind speed is 3000 km/s. Densities are given in particles per cubic centimeter.

$\dot{m}_1/(M_\odot/\mathrm{yr})$	$\dot{m}_2/(M_\odot/\mathrm{yr})$	t/yr	R_c/ly	R_1/ly	R_2/ly	n_2/cm^{-3}
10^{-6}	10^{-9}	3×10^5	67.7	74.2	16.4	1.7×10^{-7}
10^{-7}	10^{-9}	3×10^5	122	138	39.2	2.9×10^{-8}
10^{-8}	10^{-9}	3×10^5	239	278	106	4.0×10^{-9}
10^{-7}	10^{-8}	3×10^5	239	278	106	4.0×10^{-8}
10^{-7}	10^{-10}	3×10^5	67.7	74.2	16.4	1.7×10^{-8}
10^{-7}	10^{-9}	1.5×10^5	60.8	69.0	19.6	1.2×10^{-7}
10^{-7}	10^{-9}	4×10^5	162	184	52.3	1.7×10^{-8}

ranges from 10^{-8} to 10^{-10} solar masses per year; a typical rate has been measured to be 10^{-9} $M_\odot$/yr [203]. Thus, wind velocities of 3000 km/s are typical for winds from the accretion disk [203], whereas 30 km/s are typical for Red Giant companion stars and over-Eddington accretion.

The run time for the accretion disk wind and RG wind from either the WD or a RG donor star is constrained by the observed accretion rate from the companion star and the initial mass of the WD. Accretion will continue as long as the mass remains less than M_{Ch}, meaning 1.37 $M_\odot$. Using accretion rates of $2 \times 10^{-6,-8} M_\odot$/yr and initial WD masses of 0.6, 0.8, and 1.1 $M_\odot$ the times are $4 \times 10^{3,5}$, $3 \times 10^{3,5}$ and $1.5 \times 10^{3,5}$ years, respectively.

For long delays and high density environments, we must expect that they have left their initial cocoon. A "secondary" cocoon will be created by wind from the accretion disk or, if the donor star is a RG or the accretion is over-Eddington, from the an RG wind, or the accretion disk wind.

For explosions of M_{Ch} mass WDs, the progenitor system commonly creates low density cocoons of densities 10^{-4} particle/cm^3 with a typical scale of light years and which is surrounded by a thin shell. This explains why most SNe Ia appear to explode in low density environment although SN Ia are observed in the galactic halo, the disk and the bulge.

In the following, we want to address some connection between observables and the properties of a supernovae which depends on the details of the progenitor system. For high accretion rates, we expect some interaction with the rapidly expanding, outer layers of a SNe Ia within 1 to 10 years because the fastest material expands in excess of 30 000 km/s. Because the high velocity layers of SNe Ia contain $10^{48...49}$ erg [49] the impact may be seen in X-rays and may provide additional luminosity to late time light curves.

Depending on the distance of the shell from the supernovae, dust in the shell may be formed at larger distances, or destroyed for compact shells within $\approx$ 0.1 to 0.3 light years because the LC is sufficiently bright to evaporate dust. At larger distances, dust in the shell may appear as light echos. Shell at smaller distances may harbor dust with unusual properties and extinction laws which change with time.

Typically, high density shells are formed at the edge of the cocoons whose typical shell velocities are of the order of 10 to 100 km/s, which, in some cases, may give rise to narrow NaI absorption lines in the SN spectra which may vary on time scales of months [199, 204]. In the rare case that an SNe Ia progenitor is exploding in low density ISM and is within its first-generation Cocoon, we may see a very narrow, highly time variable Na I line. Nature may be more complicated. E.g. the progenitor mass loss may come in phases, namely brief periods of super-winds, and wind may not be spherical. Obviously, detailed calculations for spectra and light curves are needed to quantify the intensity of the NaI component. Radiation pressure of the SNe Ia light may accelerate nearby shells (as seen in, e.g. SN1993j). The high energy photons may trigger dust and molecule formation in the high density shells because even small charges increase the rates by orders of magnitude. Finally we need an observational data base of many supernovae to probe their statistical nature of the environment.

7 Conclusions

To first order, the outcome of a thermonuclear explosion

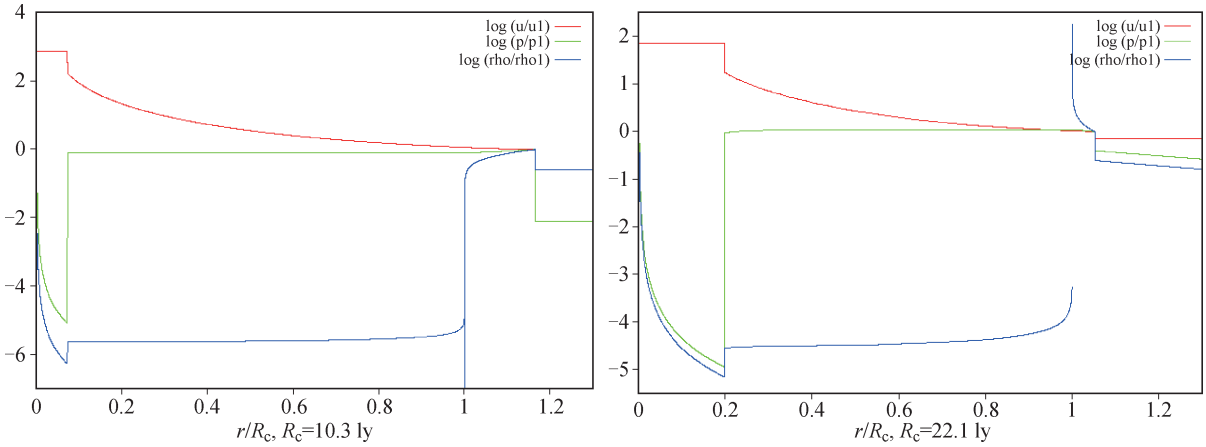

Fig. 17 Typical structures for Hydrodynamic profile for an isotropic wind of 3000 km/s and mass-loss rate of 10^{-10} $M_\odot$/yr running into a constant interstellar medium density of 1 particle/cm^3 after a time of 400 000 years (*left*) and running into a red-giant wind proportional r^{-2} density profile given by $\dot{m} = 10^{-6}$ $M_\odot$/yr and $v_w = 30$ km/s after a time of 150 000 years (*right*), respectively. The contact discontinuity are at 10.3 and 22.1 lyrs, respectively. The values for velocity (*red*), pressure (*green*), and density (*blue*) are normalized to their respective values just inside the outer shock before taking the logarithm.

of a WD hardly depends on details of the physics or scenario, or the progenitor evolution ("stellar amnesia"). Qualitatively, the general the properties of SNe Ia can be understood in terms of basic nuclear physics which determines the structure of the WD, the energy release and the light curves and spectra. Within simple physical concepts, we can understand the basic properties of LCs including the brigthness-decline relation. These concepts hold valid even for odd-balls like SN 2001ay which shows an "anti-Phillips" relation and may represent a new regime of solutions rather than a new class of explosions (Section 5). Spectra allow to map the distribution of elements in the projected velocity space and, in principle, the time evolution allows one to decypher the structure of the envelope.

With recent advances in theory and observations, direct connections emerge between the progenitor systems and their properties, and the observed light curves and spectra. However, within an increasing number of well observed SNe Ia, it also becomes increasingly obvious that SNe Ia are not "all the same".

Most likely, progenitiors include both close binary systems with an envolved compagnion star (SD), or a binary system consisting of two WDs, so called DD systems. For the explosion mechanism, the most likely candidates are off-center delayed-detonation models of a M_{Ch} mass WD which originates from an SD or DD systems in which the low mass WD is tidally disrupted and forms an accretion disk, or dynamical mergers in which two WD merge on a dynamical timescale.

In Section 6, we disussed possible signatures of the environment directly related to the progenitor system. The general lack of evidence for an ongoing interation indicates a low density in the environment of SNe Ia much lower than the ISM in the galactic disk. In DD systems, the low density can be expected because the long evolutionary time scales leads far away from the galactic disk. However, all SD progenitor systems too can be expected to form a low density cocoon of several light years surrounded by a thin shell expanding with velocities of 10 to 100 km/s. In SD progenitors, this cocoons can be formed by winds from the WD e.g. by nova outbursts or over-Eddington accretion, an accretion disk or the donor star. In several supernovae, narrow ISM lines have been observed in high resolution spectra consistent with the overall picture. Often, more than one component has been seen strongly suggesting periodic phases of high mass loss.

The majority of SNe Ia seems to come from explosions with high central densities which undergoes electron capture. Consistent evidence comes from individual light curves, namely the peak to tail ratio, IR-spectra and direct imaging of the SNR *S*-Andromeda, and statistical properties such as a narrow Δm_{15}. Moreover, most but not all, SNe Ia show little Carbon in the spectra as expected for dynamical mergers as discussed in Section 1. Moreover, continuum polarization seems to be low in SNeIa [90, 91, 205, 206] whereas we may expect strong asymmetries in dynamical mergers 1. These points combined strongly towards explosions of M_{Ch} mass WDs.

However, we have a complete set of diagnostics only for a very small number of individual objects. For example, SN2005ke shows some continuum polarization and its light curves and spectra are consistent with a M_{Ch} mass explosion but for a rapidly rotating WD [91]. However, without late time IR spectra, it was not possible to distinguish the former scenario from a dynamical merger. As discussed in Section 3, dynamical mergers may show to the signatures of M_{MS}, and the ρ_c signature may be mimiced by asphericity effects. The current analysis of the CSP data may not catch all mergers as a separate group without polarization, and pre-maximum spectra to put limits on Carbon, or late time IR-spectra. Time series of late time spectra may be needed to distinguish ionization effects from isotopic signatures.

Based on the analysis of the CSP supernovae Section 3, most of the exploding WDs come from the high mass range with main sequence masses between 3 and 7 $M_{\odot}$, and around metallicities of 0.5 to 1. times solar. However, there is a hint that 91bg-like events show a systematically lower Z hinting towards a long delay time between star formation and the explosion. Within the picture of M_{Ch} mass SNe Ia, they seem to originate from a wide range of central densities and, thus, accretion rates. With the current templates, we cannot rule out off-center ^{56}Ni distributions as an additional factor [49, 51, 54, 90], nor can we exclude that the current distribution is not an orientation effect of mergers seen from random directions.

Late time IR-spectra suggest small free mean path of positrons even after 300–400 days which suggest magnetic fields of 10^6 or above. Fields of this size can be expected to influence the dynamics and pre-conditioning of explosion. High magnetic fields may be inherented from the progenitor, or created by the dynamo mechanism during the final phase of the runaway in a M_{Ch} mass WD.

Finally, we also would like to mention the current limits which will improve in the future. Currently, high precision light curves and high resolution spectra are available for a very limited number of supernovae. Moreover, the secondary parameters reduce the residuals of the light curves by an order of magnitude but the model predictions need to be tested with supernovae in the Hubble flow. Moreover, comprehensive studies of individual supernovae are needed which include high-precision light curves, good time coverage by flux and polaria-

tion spectra and late time IR. Ongoing and upcoming projects will redeem this situation and allow statistical samples, and cross correlations between the properties of SN and their host galaxies.

Acknowledgements We would like to thank many colleges and collaborators for their support, in particular, E. Baron, R. Fesen, A. Khokhlov, M. Phillips, N. Suntzeff, L. Wang, J. C. Wheeler and many observers to provide insights and data. The work presented in this paper has been supported by the NSF projects AST-0708855, "Three-Dimensional Simulations of Type Ia Supernovae: Constraining Models with Observations" and AST-1008962, "Interaction of Type Ia Supernovae with their Environment". In parts, the results presented have been obtained in course of four PhD theses at Florida State University. The authors are especially grateful to the members of the Carnegie Supernova Project team and our NSF collaboration.

References and notes

1. F. Hoyle and W. A. Fowler, Astrophys. J., 1960, 132: 565
2. R. F. Webbink, Astrophys. J., 1984, 277: 355
3. Iben, Jr. and A. V. Tutukov, Astrophys. J. Suppl., 1984, 54: 335
4. W. Benz, A. G. W. Cameron, W. H. Press, and R. L. Bowers, Astrophys. J., 1990, 348: 647
5. F. A. Rasio and S. L. Shapiro, Astrophys. J., 1994, 432: 242
6. P. Höflich and A. Khokhlov, Astrophys. J., 1996, 457: 500
7. L. Segretain, G. Chabrier, and R. Mochkovitch, Astrophys. J., 1997, 481(1): 355
8. Z. Han and P. Podsiadlowski, Mon. Not. R. Astron. Soc., 2004, 350(4): 1301
9. S.-C. Yoon, P. Podsiadlowski, and S. Rosswog, Mon. Not. R. Astron. Soc., 2007, 380(3): 933
10. B. Wang, X.-D. Li, and Z.-W. Han, Mon. Not. R. Astron. Soc., 2010, 401(4): 2729
11. B. Wang and Z. Han, Mon. Not. R. Astron. Soc., 2010, 404(1): L84
12. R. Pakmor, S. Hachinger, F. K. Röpke, and W. Hillebrandt, Astron. Astrophys., 2011, 528: A117
13. P. Lorén-Aguilar, J. Isern, and E. Garca-Berro, Astron. Astrophys., 2009, 500: 1193
14. J. Isern, M. Hernanz, and J. José, in: Lecture Notes in Physics, Volume 812 of Lecture Notes in Physics, edited by R. Diehl, D. H. Hartmann, and N. Prantzos, Berlin: Springer-Verlag, 2011: 233
15. J. Whelan and I. J. Iben, Astrophys. J., 1973, 186: 1007
16. L. Piersanti, S. Gagliardi, Iben, Jr., and A. Tornamb, Astrophys. J., 2003, 598(2): 1229
17. J. Greiner, G. Hasinger, and P. Kahabka, Astron. Astrophys., 1991, 246: L17
18. E. P. J. van den Heuvel, D. Bhattacharya, K. Nomoto, and S. A. Rappaport, Astron. Astrophys., 1992, 262: 97
19. S. Rappaport, E. Chiang, T. Kallman, and R. Malina, Astrophys. J., 1994, 431: 237
20. P. Kahabka and E. P. J. van den Heuvel, Annu. Rev. Astron. Astrophys., 1997, 35(1): 69
21. P. F. L. Maxted, T. R. Marsh, and R. C. North, Mon. Not. R. Astron. Soc., 2000, 317(3): L41
22. P. Ruiz-Lapuente, F. Comeron, J. Mndez, R. Canal, S. J. Smartt, A. V. Filippenko, R. L. Kurucz, R. Chornock, R. J. Foley, V. Stanishev, and R. Ibata, Nature, 2004, 431(7012): 1069
23. J. I. González Hernández, P. Ruiz-Lapuente, A. V. Filippenko, R. J. Foley, A. Gal-Yam, and J. D. Simon, Astrophys. J., 2009, 691: 1
24. W. E. Kerzendorf, B. P. Schmidt, M. Asplund, K. Nomoto, P. Podsiadlowski, A. Frebel, R. A. Fesen, and D. Yong, Astrophys. J., 2009, 701(2): 1665
25. B. E. Schaefer and A. Pagnotta, Nature, 2012, 481(7380): 164
26. Z. I. Edwards, A. Pagnotta, and B. E. Schaefer, Astrophys. J., 2012, 747(2): L19
27. B. Wang, X. Meng, X. Chen, and Z. Han, Mon. Not. R. Astron. Soc., 2009, 395(2): 847
28. B. Wang, X. Chen, X. Meng, and Z. Han, Astrophys. J., 2009, 701(2): 1540
29. D. Maoz, Mon. Not. R. Astron. Soc., 2008, 384(1): 267
30. D. Maoz, K. Sharon, and A. Gal-Yam, Astrophys. J., 2010, 722(2): 1879
31. D. Maoz, F. Mannucci, W. Li, A. V. Filippenko, M. Della Valle, and N. Panagia, Mon. Not. R. Astron. Soc., 2011, 412(3): 1508
32. H. Saio and K. Nomoto, Astrophys. J., 1998, 500(1): 388
33. S. E. Woosley and T. A. Weaver, in: NATO ASIC Proc. 163: Nucleosynthesis and its Implications on Nuclear and Particle Physics, edited by J. Audouze and N. Mathieu, 1986: 145
34. R. Mochkovitch and M. Livio, Astron. Astrophys., 1990, 236: 378
35. H. Saio and K. Nomoto, Astron. Astrophys., 1985, 150: L21
36. K. J. Shen, L. Bildsten, D. Kasen, and E. Quataert, Astrophys. J. (in press), arXiv: astro-ph/1108.4036, 2011
37. D. Branch, M. Livio, L. R. Yungelson, F. R. Boffi, and E. Baron, Publ. Astron. Soc. Pac., 1995, 107: 1019
38. K. Nomoto, T. Uenishi, C. Kobayashi, H. Umeda, T. Ohkubo, I. Hachisu, and M. Kato, in: From Twilight to Highlight: The Physics of Supernovae, edited by W. Hillebrandt and B. Leibundgut, 2003: 115
39. B. Wang and Z. Han, New Astron. Rev., 2012, 56(4): 122
40. R. Di Stefano, R. Voss, and J. S. W. Claeys, in: AAS/High Energy Astrophysics Division, volume 12 of AAS/High Energy Astrophysics Division, 2011: 33.04
41. R. Di Stefano and M. Kilic, arXiv: 1205.3168 [astro-ph.SR], 2012
42. S. Benetti, P. Meikle, M. Stehle, G. Altavilla, S. Desidera, G. Folatelli, A. Goobar, S. Mattila, J. Mendez, H. Navasardyan, A. Pastorello, F. Patat, M. Riello, P. Ruiz-Lapuente, D. Tsvetkov, M. Turatto, P. Mazzali, and W. Hillebrandt, Mon. Not. R. Astron. Soc., 2004, 348(1): 261

43. D. A. Howell, M. Sullivan, P. E. Nugent, R. S. Ellis, et al., Nature, 2006, 443: 308
44. R. Quimby, P. Höflich, S. J. Kannappan, E. Rykoff, W. Rujopakarn, C. W. Akerlof, C. L. Gerardy, and J. C. Wheeler, Astrophys. J., 2006, 636(1): 400
45. M. Yamanaka, K. S. Kawabata, K. Kinugasa, M. Tanaka, et al., Astrophys. J., 2009, 707(2): L118
46. F. K. Röpke, M. Kromer, I. R. Seitenzahl, R. Pakmor, et al., Astrophys. J., 2012, 750(1): L19
47. S. Hachinger, P. A. Mazzali, S. Taubenberger, M. Fink, R. Pakmor, W. Hillebrandt, and I. R. Seitenzahl, arXiv: 1209.1339 [astro-ph.SR], 2012
48. D. Branch, Publ. Astron. Soc. Pac., 2001, 113(780): 169
49. P. Höflich, Nucl. Phys. A., 2006, 777: 579
50. P. Höflich, C. L. Gerardy, K. Nomoto, K. Motohara, R. A. Fesen, K. Maeda, T. Ohkubo, and N. Tominaga, Astrophys. J., 2004, 617(2): 1258
51. K. Motohara, K. Maeda, C. L. Gerardy, K. Nomoto, M. Tanaka, N. Tominaga, T. Ohkubo, P. A. Mazzali, R. A. Fesen, P. Höflich, and J. C. Wheeler, Astrophys. J., 2006, 652(2): L101
52. R. A. Fesen, P. A. Höflich, A. J. S. Hamilton, M. C. Hammell, C. L. Gerardy, A. M. Khokhlov, and J. C. Wheeler, Astrophys. J., 2007, 658(1): 396
53. C. L. Gerardy, P. Höflich, R. A. Fesen, G. H. Marion, K. Nomoto, R. Quimby, B. E. Schaefer, L. Wang, and J. C. Wheeler, Astrophys. J., 2004, 607(1): 391
54. K. Maeda, S. Benetti, M. Stritzinger, F. K. Röpke, G. Folatelli, J. Sollerman, S. Taubenberger, K. Nomoto, G. Leloudas, M. Hamuy, M. Tanaka, P. A. Mazzali, and N. Elias-Rosa, Nature, 2010, 466(7302): 82
55. A. M. Khokhlov, Astron. Astrophys., 245: L25, 1991
56. S. E. Woosley and T. A. Weaver, Astrophys. J., 1994, 423: 371
57. H. Yamaoka, K. Nomoto, T. Shigeyama, and F. K. Thielemann, Astrophys. J., 1992, 393: L55
58. P. Höflich, Astrophys. J., 1995, 443: 89
59. P. Höflich, A. M. Khokhlov, and J. C. Wheeler, Astrophys. J., 1995, 444: 831
60. A. Fisher, D. Branch, P. Nugent, and E. Baron, Astrophys. J., 1997, 481(2): L89
61. P. E. Nugent, Non-Local Thermodynamic Equilibrium Spectrum Synthesis of Type IA Supernovae, PhD thesis, The University of Oklahoma, 1997
62. J. C. Wheeler, P. Hoeflich, R. P. Harkness, and J. Spyromilio, Astrophys. J., 1998, 496(2): 908
63. E. J. Lentz, E. Baron, D. Branch, and P. H. Hauschildt, Astrophys. J., 2001, 557(1): 266
64. V. N. Gamezo, A. M. Khokhlov, E. S. Oran, A. Y. Chtchelkanova, and R. O. Rosenberg, Science, 2003, 299(5603): 77
65. V. N. Gamezo, A. M. Khokhlov, and E. S. Oran, Astrophys. J., 2005, 623(1): 337
66. A. Y. Poludnenko, T. A. Gardiner, and E. S. Oran, Phys. Rev. Lett., 2011, 107(5): 054501
67. R. Barbon, S. Benetti, L. Rosino, E. Cappellaro, and M. Turatto, Astron. Astrophys., 1990, 237: 79
68. P. Höflich, C. Gerardy, R. Fesen, and S. Sakai, Astrophys. J., 2002, 568(2): 791
69. M. Stehle, P. A. Mazzali, S. Benetti, and W. Hillebrandt, Mon. Not. R. Astron. Soc., 2005, 360(4): 1231
70. M. M. Phillips, Astrophys. J., 1993, 413: L105
71. M. M. Phillips, P. Lira, N. B. Suntzeff, R. A. Schommer, M. Hamuy, and J. Maza, Astron. J., 1999, 118(4): 1766
72. G. Goldhaber, D. E. Groom, A. Kim, G. Aldering, et al., Astrophys. J., 2001, 558(1): 359
73. S. A. Colgate and C. McKee, Astrophys. J., 1969, 157: 623
74. P. Höflich, A. Khokhlov, J. C. Wheeler, M. M. Phillips, N. B. Suntzeff, and M. Hamuy, Astrophys. J., 1996, 472(2): L81
75. P. Nugent, E. Baron, D. Branch, A. Fisher, and P. Hauschildt, Astrophys. J., 1997, 485(2): 812
76. H. Umeda, K. Nomoto, C. Kobayashi, I. Hachisu, and M. Kato, Astrophys. J., 1999, 522(1): L43
77. D. Kasen, F. K. Röpke, and S. E. Woosley, Nature, 2009, 460(7257): 869
78. E. Baron, P. Höflich, K. Krisciunas, I. Dominguez, A. M. Khokhlov, M. M. Phillips, N. Suntzeff, and L. Wang, Astrophys. J., 2012, 753(2): 105
79. M. Hamuy, et al., Astron. J., 1996, 112: L81
80. A. G. Riess, W. H. Press, and R. P. Kirshner, Astrophys. J., 1996, 473(1): 88
81. N. B. Suntzeff, M. M. Phillips, R. Covarrubias, M. Navarrete, J. Prez, A. Guerra, M. T. Acevedo, L. R. Doyle, T. Harrison, S. Kane, and K. S. Long, Astron. J., 1999, 117: 1175
82. S. Perlmutter, M. Turner, and M. White, Phys. Rev. Lett., 1999, 83(4): 670
83. P. Höflich, K. Krisciunas, A. M. Khokhlov, E. Baron, G. Folatelli, M. Hamuy, M. M. Phillips, N. Suntzeff, and L. Wang, Astrophys. J., 2010, 710(1): 444
84. F. K. Röpke, W. Hillebrandt, J. C. Niemeyer, and S. E. Woosley, Astrophys., 2006, 448: 1
85. P. Höflich, J. C. Wheeler, and F. K. Thielemann, Astrophys. J., 1998, 495(2): 617
86. E. Lentz, E. Baron, D. Branch, P. H. Hauschildt, and P. Nugent, Astrophys. J., 2000, 530(2): 966
87. D. A. Howell, P. Höflich, L. Wang, and J. C. Wheeler, Astrophys. J., 2001, 556: 302
88. S. C. Yoon and N. Langer, Astron. Astrophys., 2004, 419(2): 623
89. S. C. Yoon and N. Langer, in: Cosmic explosions in three dimensions, edited by P. Höflich, P. Kumar, and J. C. Wheeler, 2004: 94
90. J. R. Maund, P. A. Hoeflich, F. Patat, J. C. Wheeler, P. Zelaya, D. Baade, L. Wang, A. Clocchiatti, and J. Quinn, Astrophys. J., 2010, 725(2): L167
91. F. Patat, P. Höflich, D. Baade, J. R. Maund, L. Wang, and J. C. Wheeler, Astron. Astrophys., 2012, 545: A7
92. P. Höflich and J. Stein, Astrophys. J., 2002, 568(2): 779

93. G. Tovmassian and E. Sion (Eds.), A circumstellar interaction model for SN 2002IC, volume 20 of Revista Mexicana de Astronomia y Astrofisica Conference Series, 2004
94. T. Uenishi, K. Nomoto, and I. Hachisu, Nucl. Phys. A., 2003, 718: 623
95. A. C. Calder, T. Plewa, N. Vladimirova, D. Q. Lamb, J. W. Truran, arXiv: astro-ph/0405162, 2004
96. E. Livne, S. M. Asida, and P. Höflich, Astrophys. J., 2005, 632(1): 443
97. D. Kasen and T. Plewa, Astrophys. J., 2005, 21(1): L41
98. D. Kasen and T. Plewa, Astrophys. J., 2007, 662(1): 459
99. F. K. Röpke, S. E. Woosley, and W. Hillebrandt, Astrophys. J., 2007, 660(2): 1344
100. S. A. Sim, D. N. Sauer, F. K. Röpke, and W. Hillebrandt, Mon. Not. R. Astron. Soc., 2007, 378(1): 2
101. I. R. Seitenzahl, C. A. Meakin, D. Q. Lamb, and J. W. Truran, Astrophys. J., 2009, 700(1): 642
102. M. Zingale, A. S. Almgren, J. B. Bell, A. Nonaka, and S. E. Woosley, Astrophys. J., 2009, 704(1): 196
103. R. A. Scalzo, G. Aldering, P. Antilogus, C. Aragon, et al., Astrophys. J., 2010, 713(2): 1073
104. S. Taubenberger, S. Benetti, M. Childress, R. Pakmor, et al., Mon. Not. R. Astron. Soc., 2011, 412: 2735, arXiv: 1011.5665 [astro-ph.SR]
105. D. A. Howell, Nat. Commun., 2, 2011.
106. W. R. Hix and F. K. Thielemann, J. Comput. Appl. Math., 1999, 109(1–2): 321
107. A. Khokhlov, Astron. Astrophys., 1991, 245: 114
108. A. M. Khokhlov, E. S. Oran, and J. C. Wheeler, Astrophys. J., 1997, 478(2): 678
109. J. C. Niemeyer and S. E. Woosley, Astrophys. J., 1997, 475(2): 740
110. E. Livne, Astrophys. J., 1999, 527(2): L97
111. D. J. Jeffery, B. Leibundgut, R. P. Kirshner, S. Benetti, D. Branch, and G. Sonneborn, Astrophys. J., 1992, 397: 304
112. R. P. Kirshner, D. J. Jeffery, B. Leibundgut, P. M. Challis, et al., Astrophys. J., 1993, 415: 589
113. G. H. Marion, P. Höflich, W. D. Vacca, and J. C. Wheeler, Astrophys. J., 2003, 591(1): 316
114. M. Stritzinger, M. Hamuy, N. B. Suntzeff, R. C. Smith, M. M. Phillips, J. Maza, L. G. Strolger, R. Antezana, L. Gonzlez, M. Wischnjewsky, P. Candia, J. Espinoza, D. Gonzlez, C. Stubbs, A. C. Becker, E. P. Rubenstein, and G. Galaz, Astron. J., 2002, 124(4): 2100
115. L. G. Strolger, R. C. Smith, N. Suntzeff, B. Schommer, M. Phillips, L. Ho, E. Rubenstein, M. Hamuy, R. Covarrubias, A. Clocchiatti, and M. Maza, in: American Astronomical Society Meeting Abstracts, volume 31 of Bulletin of the American Astronomical Society, 1999: 1423
116. P. M. Garnavich, A. Z. Bonanos, K. Krisciunas, S. Jha, R. P. Kirshner, E. M. Schlegel, P. Challis, L. M. Macri, K. Hatano, D. Branch, G. D. Bothun, and W. L. Freedman, Astrophys. J., 2004, 613(2): 1120
117. R. Harkness, in: IAU Colloq. 89: Radiation Hydrodynamics in Stars and Compact OAJects, volume 255 of Lecture Notes in Physics, edited by D. Mihalas and K.-H. A. Winkler, Berlin: Springer-Verlag, 1986: 166
118. P. Mazzali, E. Cappellaro, I. Danziger, M. Turatto, and S. Benetti, Astrophys. J., 1998, 499(1): L49
119. G. Goldhaber and S. Perlmutter, Phys. Rep., 1998, 307(1-4): 325
120. A. Riess, A. V. Filippenko, W. Li, and B. P. Schmidt, Astron. J., 1999, 118(6): 2668
121. S. Perlmutter, G. Aldering, G. Goldhaber, R. A. Knop, et al., Astrophys. J., 1999, 517(2): 565
122. A. Riess, A. V. Filippenko, P. Challis, A. Clocchiatti, et al., Astron. J., 1998, 116(3): 1009
123. D. Branch, Annu. Rev. Astron. Astrophys., 1999, 36: 579
124. F. Brachwitz, D. J. Dean, W. R. Hix, K. Iwamoto, and K. Langanke, Astrophys. J., 2000, 536: 934
125. D. Kasen, P. Nugent, L. Wang, D. A. Howell, J. C. Wheeler, P. Höflich, D. Baade, E. Baron, and P. Hauschildt, Astrophys. J., 2003, 593(2): 788
126. P. Höflich, C. L. Gerardy, H. Marion, and R. Quimby, New Astron. Rev., 2006, 50(7–8): 470
127. C. Contreras, M. Hamuy, M. M. Phillips, G. Folatelli, et al.,Astron. J., 2010, 139(2): 519
128. G. Folatelli, M. M. Phillips, C. R. Burns, C. Contreras, et al., Astron. J., 2010, 139: 120
129. M. D. Stritzinger, M. M. Phillips, L. N. Boldt, C. Burns, et al., Astron. J., 2011, 142(5): 156
130. M. Hicken, P. Challis, S. Jha, R. P. Kirshner, et al., Astrophys. J., 2009, 700(1): 331
131. G. Aldering, G. Adam, P. Antilogus, P. Astier, et al., Overview of the Nearby Supernova Factory, in: Society of Photo-Optical Instrumentation Engineers (SPIE) Conference Series, volume 4836 of Society of Photo-Optical Instrumentation Engineers (SPIE) Conference Series, edited by J. A. Tyson and S. Wolff, 2002: 61
132. B. Sadler, Constraining Type Ia Supernovae Progenitors by Light Curves, Ph.D. thesis, Florida State University, 2012
133. K. Hatano, D. Branch, E. J. Lentz, E. Baron, A. V. Filippenko, and P. M. Garnavich, Astrophys. J., 2000, 543(1): L49
134. F. X. Timmes, E. F. Brown, and J. W. Truran, Astrophys. J., 2003, 590(2): L83
135. K. Sadler, P. Höflich, E. Baron, K. Krisciunas, G. Folatelli, M. Hamuy, A. M. Khokhlov, M. M. Phillips, N. B. Suntzeff, and L. Wang, In: Binary Paths to SNeIa Explosions, volume 281 of IAU Symposium, edited by R. DiStephano and M. Orio, 2012
136. P. Höflich, K. Krisciunas, A. M. Khokhlov, E. Baron, G. Folatelli, M. Hamuy, M. M. Phillips, N. Suntzeff, and L. Wang, arXiv: 0912.2231 [astro-ph.CO], 2009
137. C. R. Burns, M. Stritzinger, M. M. Phillips, S. Kattner, S. E. Persson, B. F. Madore, W. L. Freedman, L. Boldt, A. Campillay, C. Contreras, G. Folatelli, S. Gonzalez, W.

Krzeminski, N. Morrell, F. Salgado, and N. B. Suntzeff, Astron. J., 2011, 141(1): 19

138. E. Y. Hsiao, A. Conley, D. A. Howell, M. Sullivan, C. J. Pritchet, R. G. Carlberg, P. E. Nugent, and M. M. Phillips, Astrophys. J., 2007, 663(2): 1187
139. J. Nelder and R. Mead, Comput. J., 1965, 7(4): 308
140. S. Jha, R. P. Kirshner, P. Challis, P. M. Garnavich, et al., Astron. J., 2006, 131(1): 527
141. P. Höflich, K. Nomoto, H. Umeda, and J. C. Wheeler, Astrophys. J., 2000, 528(2): 590
142. I. Dom nguez, P. Höflich, and O. Straniero, Astrophys. J., 2001, 557: 279
143. P. Höflich, Astron. Astrophys., 1991, 246: 481
144. K. Maeda, G. Leloudas, S. Taubenberger, M. Stritzinger, J. Sollerman, N. Elias-Rosa, S. Benetti, M. Hamuy, G. Folatelli, and P. A. Mazzali, Mon. Not. R. Astron. Soc., 2011, 413(4): 3075
145. R. Fesen, C. L. Gerardy, A. V. Filippenko, T. Matheson, R. A. Chevalier, R. P. Kirshner, B. P. Schmidt, P. Challis, C. Fransson, B. Leibundgut, and S. D. Van Dyk, Astron. J., 1999, 117(2): 725
146. A. J. S. Hamilton and R. A. Fesen, Astrophys. J., 2000, 542(2): 779
147. R. A. Fesen, in: Cosmic Explosions in Three Dimensions, edited by P. Höflich, P. Kumar, and J. C. Wheeler, Cambridge: Cambridge University Press, 2005: 64
148. R. W. Bussard, R. Ramaty, and R. J. Drachman, Astrophys. J., 1979, 228: 928
149. B. L. Brown and M. Leventhal, Astrophys. J., 1987, 319: 637
150. S. Colgate, A. Petschek, and J. Kriese, Astrophys. J., 1980, 237: L81
151. K. W. Chan and R. E. Lingenfelter, Astrophys. J., 1993, 405: 614
152. P. A. Milne, L.-S. The, and M. D. Leising, Astrophys. J. Suppl., 1999, 124(2): 503
153. R. Penney, Techniques for Probing Effects of MHD in SNe Ia, PhD thesis, Florida State University, 2011
154. B. Penny, P. Höflich, and C. Gerardy, Astrophys. J., 2012
155. E. J. C. Bowers, W. P. S. Meikle, T. R. Geballe, N. A. Walton, P. A. Pinto, V. S. Dhillon, S. B. Howell, and M. K. Harrop-Allin, Mon. Not. R. Astron. Soc., 1997, 290(4): 663
156. M. Zingale, S. E. Woosley, C. Rendleman, M. Day, and J. Bell, Astrophys. J., 2005, 632(2): 1021
157. W. Li, J. S. Bloom, P. Podsiadlowski, A. A. Miller, et al., Nature, 2011, 480(7377): 348
158. E. Müller, P. Höflich, and A. Khokhlov, Astron. Astrophys., 1991, 249: L1
159. A. Saha, A. Sandage, G. A. Tammann, L. Labhardt, F. D. Macchetto, and N. Panagia, Astrophys. J., 1999, 522(2): 802
160. M. M. Phillips, L. A. Wells, N. B. Suntzeff, M. Hamuy, B. Leibundgut, R. P. Kirshner, and C. B. Foltz, Astron. J., 1992, 103: 1632
161. P. Ruiz-Lapuente, E. Cappellaro, M. Turatto, C. Gouiffes, I. J. Danziger, M. Della Valle, and L. B. Lucy, Astrophys. J., 1992, 387: L33
162. K. Krisciunas, N. B. Suntzeff, M. M. Phillips, P. Candia, et al., Astron. J., 2004, 128(6): 3034
163. P. Mazzali, I. J. Danziger, and M. Turatto, Astron. Astrophys., 1995, 297: 509
164. W. Liu, D. J. Jeffery, and D. R. Schultz, Astrophys. J., 1997, 486(1): L35
165. K. Krisciunas, W. Li, T. Matheson, D. A. Howell, et al., Astron. J., 2011, 142(3): 74
166. K. Krisciunas, E. Baron, P. Höflich, A. M. Khokhlov, I. Dominguez, L. Wang, N. B. Suntzeff, M. Hamuy, and M. M. Phillips, in: American Astronomical Society Meeting Abstracts 218, 2011: 127.06
167. W. D. Arnett, Astrophys. J., 1982, 253: 785
168. M. Hamuy, M. M. Phillips, N. B. Suntzeff, J. Maza, L. E. Gonzlez, M. Roth, K. Krisciunas, N. Morrell, E. M. Green, S. E. Persson, and P. J. McCarthy, Nature, 2003, 424(6949): 651
169. E. J. Lentz, E. Baron, P. H. Hauschildt, and D. Branch, Astrophys. J., 2002, 580(1): 374
170. M. Livio and A. G. Riess, Astrophys. J., 2003, 594(2): L93
171. Z. Han and P. Podsiadlowski, Mon. Not. R. Astron. Soc., 2006, 368(3): 1095
172. G. Aldering, P. Antilogus, S. Bailey, C. Baltay, et al., Astrophys. J., 2006, 650(1): 510
173. E. Marietta, A. Burrows, and B. Fryxell, Astrophys. J. Suppl., 128:615, 2000.
174. R. Quimby, P. Höflich, and J. C. Wheeler, Astrophys. J., 2007, 666(2): 1083
175. A. Fisher, Direct Analysis of Type Ia Supernovae, Ph.D. thesis, University of Oklahoma, 2000 (unpublished)
176. L. Wang, D. Baade, P. Höflich, A. Khokhlov, J. C. Wheeler, D. Kasen, P. E. Nugent, S. Perlmutter, C. Fransson, and P. Lundqvist, Astrophys. J., 2003, 591(2): 1110
177. N. N. Chugai, Sov. Astron., 1986, 30: 563
178. E. M. Schlegel and R. Petre, Astrophys. J., 1993, 412: L29
179. E. M. Schlegel, Rep. Prog. Phys., 1995, 58(11): 1375
180. R. J. Cumming, P. Lundqvist, L. J. Smith, M. Pettini, and D. L. King, Mon. Not. R. Astron. Soc., 1996, 283: 1355
181. L. Chomiuk, A. M. Soderberg, M. Moe, R. A. Chevalier, M. P. Rupen, C. Badenes, R. Margutti, C. Fransson, W. F. Fong, and J. A. Dittmann, Astrophys. J., 2012, 750(2): 164
182. B. P. Schmidt, R. P. Kirshner, B. Leibundgut, L. A. Wells, A. C. Porter, P. Ruiz-Lapuente, P. Challis, and A. V. Filippenko, Astrophys. J., 1994, 434: L19
183. L. Wang, P. Höflich, and J. C. Wheeler, Astrophys. J., 1997, 483(1): L29
184. K. M. Ferrière, Rev. Mod. Phys., 2001, 73(4): 1031
185. J. A. Cardelli, G. C. Clayton, and J. S. Mathis, Astrophys. J., 1989, 345: 245

186. K. Krisciunas, N. C. Hastings, K. Loomis, R. McMillan, A. Rest, A. G. Riess, and C. Stubbs, Astrophys. J., 2000, 539(2): 658

187. N. Elias-Rosa, S. Benetti, E. Cappellaro, M. Turatto, et al., Mon. Not. R. Astron. Soc., 2006, 369(4): 1880

188. J. Nordin, Astrophys. J., 2011, 734: 42

189. A. Pastorello, S. Benetti, F. Bufano, E. Kankare, S. Mattila, M. Turatto, and G. Cupani, Astron. Nachr., 2011, 332(3): 266

190. M. Hamuy, S. C. Trager, P. A. Pinto, M. M. Phillips, R. A. Schommer, V. Ivanov, and N. B. Suntzeff, Astron. J., 2000, 120(3): 1479

191. A. Rest, N. B. Suntzeff, K. Olsen, J. L. Prieto, R. C. Smith, D. L. Welch, A. Becker, M. Bergmann, A. Clocchiatti, K. Cook, A. Garg, M. Huber, G. Miknaitis, D. Minniti, S. Nikolaev, and C. Stubbs, Nature, 2005, 438(7071): 1132

192. F. Patat, S. Benetti, S. Justham, P. A. Mazzali, L. Pasquini, E. Cappellaro, and M. Della Valle, P. Podsiadlowski, M. Turatto, A. Gal-Yam, and J. D. Simon, Astron. Astrophys., 2007, 474: 931

193. A. P. S. Crotts and D. Yourdon, Astrophys. J., 2008, 689(2): 1186

194. X. Wang, W. Li, A. V. Filippenko, R. J. Foley, N. Smith, and L. Wang, Astrophys. J., 2008, 677(2): 1060

195. A. Rest, T. Matheson, S. Blondin, M. Bergmann, D. L. Welch, N. B. Suntzeff, R. C. Smith, K. Olsen, J. L. Prieto, A. Garg, P. Challis, C. Stubbs, M. Hicken, M. Modjaz, W. M. Wood-Vasey, A. Zenteno, G. Damke, A. Newman, M. Huber, K. H. Cook, S. Nikolaev, A. C. Becker, A. Miceli, R. Covarrubias, L. Morelli, G. Pignata, A. Clocchiatti, D. Minniti, and R. J. Foley, Astrophys. J., 2008, 680(2): 1137

196. S. D dorico, S. di Serego Alighieri, M. Pettini, P. Magain, P. E. Nissen, and N. Panagia, Astron. Astrophys., 1989, 215: 21

197. F. Patat, P. Chandra, R. Chevalier, S. Justham, et al., Science, 2007, 317(5840): 924

198. S. Blondin, J. L. Prieto, F. Patat, P. Challis, M. Hicken, R. P. Kirshner, T. Matheson, and M. Modjaz, Astrophys. J., 2009, 693(1): 207

199. R. J. Foley, J. D. Simon, C. R. Burns, A. Gal-Yam, M. Hamuy, R. P. Kirshner, N. I. Morrell, M. M. Phillips, G. A. Shields, and A. Sternberg, Astrophys. J., 2012, 752(2): 101

200. E. N. Parker, Interplanetary Dynamical Processes, 1963

201. R. A. Chevalier, Astrophys. J., 1982, 258: 790

202. P. Dragolin, P. Höflich, and A. Khokhlov, Astrophys. J., 2013 (submitted)

203. S. Kafka and R. K. Honeycutt, Astron. J., 2004, 128(5): 2420

204. A. Sternberg, A. Gal-Yam, J. D. Simon, D. C. Leonard, et al., Science, 2011, 333(6044): 856

205. L. Wang, J. C. Wheeler, Z. Li, and A. Clocchiatti, Astrophys. J., 1996, 467: 435

206. L. Wang, J. C. Wheeler, and P. Höflich, Astrophys. J. Lett., 1997, 476(1): 27